An amplitude equation for the conserved-Hopf bifurcation— Derivation, analysis, and assessment ⊘

Daniel Greve ✉ iD ; Uwe Thiele iD

Check for updates

View Online

Export Citation

Articles You May Be Interested In

KoopmanLab: Machine learning for solving complex physics equations

APL Mach. Learn. (September 2023)

Experimental realization of a quantum classification: Bell state measurement via machine learning

APL Mach. Learn. (September 2023)

An amplitude equation for the conserved-Hopf bifurcation—Derivation, analysis, and assessment

View Online   Export Citation   CrossMark

Daniel Greve[1,a)] (ID) and Uwe Thiele[1,2,3,b)] (ID)

AFFILIATIONS

[1] Institut für Theoretische Physik, Universität Münster, Wilhelm-Klemm-Str. 9, 48149 Münster, Germany
[2] Center for Nonlinear Science (CeNoS), Universität Münster, Corrensstr. 2, 48149 Münster, Germany
[3] Center for Multiscale Theory and Computation (CMTC), Universität Münster, Corrensstr. 40, 48149 Münster, Germany

[a)] Author to whom correspondence should be addressed: daniel.greve@uni-muenster.de
[b)] Electronic mail: u.thiele@uni-muenster.de

ABSTRACT

We employ weakly nonlinear theory to derive an amplitude equation for the conserved-Hopf instability, i.e., a generic large-scale oscillatory instability for systems with two conservation laws. The resulting equation represents in the conserved case the equivalent of the complex Ginzburg–Landau equation obtained in the nonconserved case as an amplitude equation for the standard Hopf bifurcation. Considering first the case of a relatively simple symmetric two-component Cahn–Hilliard model with purely nonreciprocal coupling, we derive the nonlinear nonlocal amplitude equation with real coefficients and show that its bifurcation diagram and time evolution well agree with the results for the full model. The solutions of the amplitude equation and their stability are analytically obtained, thereby showing that in such oscillatory phase separation, the suppression of coarsening is universal. Second, we lift the two restrictions and obtain the amplitude equation in the generic case. It has complex coefficients and also shows very good agreement with the full model as exemplified for some transient dynamics that converges to traveling wave states.

Nonreciprocal interactions and conservation laws both play an important role in out-of-equilibrium pattern formation processes, e.g., in biochemical systems. The generic oscillatory instability in such systems—the conserved-Hopf instability—is increasingly being studied as a central organizing element for the ongoing dynamic patterning. We employ a weakly nonlinear multi-scale analysis to obtain closed-form (but nonlocal) slow-time evolution equations for the spatiotemporal dynamics of the amplitude of fast-time oscillations for two-species Cahn–Hilliard models with nonreciprocal interactions. A comparison of analytical results for the reduced model and numerical results for the full model reveals excellent agreement. The derived amplitude equations will allow for a systematic study of universal behavior occurring in the vicinity of conserved-Hopf instabilities.

I. INTRODUCTION

For spatially extended dynamical systems, multiscale analyses represent a powerful tool to identify universal behavior close to the onset of linear instabilities, i.e., in the vicinity of local bifurcations.[1–4]

Independently of the specific system or instability, this relies on two key observations: On the one hand, the growth rates of the mode(s) destabilized at the bifurcation are small, i.e., their dynamics occurs on a much slower timescale than the one of the stable modes. The latter relax on a fast timescale implying that they are slaved to the slow modes.[5] On the other hand, in pattern forming systems, unstable modes only occur in a small band of wavenumbers about the critical one. This results in the emergence of length scales and typically results in a scale separation between the length scale of a pattern and the length scale over which its amplitude or phase are modulated.[2,3]

The ensuing scale separation in space and/or time is then employed through various multiscale expansions for systems that develop spatial structures or patterns resulting in amplitude (or envelope, or modulation) equations. These represent crucial simplifications as they are of reduced complexity with reduced order parameter and control parameter sets due to the eliminated small length and/or fast timescales. This can dramatically reduce the numerical effort. Often they even allow for analytical insights into universal behavior beyond linear approximations. Further, amplitude equations are quite valuable tools if one aims at a deeper

understanding of possible generic qualitative behaviors in classes of systems and the changes occurring with changing parameters. This then allows one, for instance, to draw parallels between seemingly unrelated physical systems, here, e.g., between reaction–diffusion systems with two conservation laws and heated two-layer liquid films. However, also note that amplitude equations are a less than ideal tool if one aims at detailed quantitative predictions of nonlinear behavior for a particular system at diverse sets of parameters far from instability onset, e.g., in biophysics or material science.

A prominent classification of instabilities in spatially extended systems by Cross and Hohenberg[2] distinguishes three types (I, II, and III) with two respective flavors: stationary (or monotonic) and oscillatory—in total, six categories of generic codimension-one instabilities. However, it has turned out that this traditional classification is not ideally suited when systematically considering systems with conservation laws that have come into sharper focus over the past two decades.[6–16]

In consequence, a recent alternative classification into eight categories is based on three dichotomous properties, namely, large-scale (L) vs small-scale (S) instability, stationary (s) vs oscillatory (o) instability, and nonconserved (N) vs conserved (C) dynamics of relevant mode(s). A table that lists the resulting eight instability types, the employed naming convention, and their relation to the traditional classification is given in the supplementary material of Ref. 16. Here, it is reproduced in Appendix A as Table II together with some further remarks.

Here, we solely focus on length and timescales that arise from the dispersion relations and their implications for the corresponding amplitude equation obtained by a weakly nonlinear approach. They are well known for the four cases without conservation law: Turing (small-scale, stationary) and Hopf (large-scale, oscillatory) instability give rise to the real and complex Ginzburg–Landau equation, respectively, that effectively describe the respective spatiotemporal modulation of harmonic spatial modulations and of harmonic temporal oscillations on large length and slow timescale. Because no fast time or small length scale is induced by the dispersion relation, in the case of the Allen–Cahn instability (large-scale, stationary), the relevant "amplitude" is a simple scalar order parameter field, resulting in the Allen–Cahn equation as "amplitude equation." In the case of a wave instability (small-scale, oscillatory), the amplitude equation corresponds to coupled complex Ginzburg–Landau equations for the amplitudes of left- and right-traveling waves. They are, however, only valid at small group velocity (see, e.g., Sec. VI E of Ref. 17). Otherwise, the amplitude equation is nonlocal.[18,19] The four basic cases without conservation law are all well covered by the Cross–Hohenberg classification and extensively analyzed in the literature.

However, this is less so for the four cases with conservation laws. There, one has to additionally account for the slow relaxation of the large-scale modes, i.e., with near-zero wavenumber. In the case of the conserved-Turing instability, the real Ginzburg–Landau equation then couples to a nonlinear diffusion equation,[6] while the case of the conserved-wave instability results in two complex Ginzburg–Landau equations coupled to a nonlinear diffusion equation.[7] The Cahn–Hilliard instability is the conserved equivalent of the Allen–Cahn instability, implying that the relevant amplitude is also a simple scalar field and the amplitude equation is a

Cahn–Hilliard equation,[20] explaining the coarsening behavior for many reaction–diffusion (RD) systems with one conservation law, in particular, in the vicinity of a large-scale stationary instability.[8,21–23]

In the final case of a conserved-Hopf instability, two conservation laws are needed to allow for a large-scale oscillatory instability of a conserved mode. Although such instabilities and the resulting nonlinear oscillatory behavior have been described for a number of systems with at least two conservation laws,[10,12,24–29] a systematic understanding of the underlying universal behavior has still to emerge. A particular case that has recently attracted considerable attention is the nonreciprocally coupled Cahn–Hilliard model.[16,30–41]

Reference 16 has shown that a general nonreciprocal two-component Cahn–Hilliard model captures the universal behavior in the vicinity of any conserved-Hopf instability in terms of the dynamics of two density-like scalar fields that directly correspond to the trivial amplitudes of the zero-modes as in the corresponding stationary case. However, although the resulting "amplitude equation" captures the corresponding behavior of many specific systems and encodes their parameters in its universal but still extremely rich parameter set, it does not correspond to an amplitude equation in the spirit of a Ginzburg–Landau-type equation that eliminates a small length or fast timescale. Actually, the equation derived in Ref. 16 instead corresponds to the amplitude equation for an instability of higher codimension because it encompasses further primary bifurcations besides the conserved-Hopf instability, e.g., a codimension-two Cahn–Hilliard instability. Therefore, the corresponding proper amplitude equation that eliminates the timescale of fast oscillations is still missing.

Our present work develops such an amplitude equation and in this way hopefully completes the set of eight such equations for the eight above discussed linear instabilities. Our approach is based on a close inspection of the dispersion relation that implies the occurrence of two different timescales (see Fig. 1). On the one hand, there are the frequencies of the unstable modes. They scale with ε^2, where ε represents the distance to the onset of the conserved-Hopf instability. On the other hand, the fastest growing unstable mode has a growth rate of order ε^4. We show that these timescales can be separated, ultimately resulting in an amplitude equation that captures the nonlinear behavior of the slowly evolving amplitude of the modes with ε^2-frequencies in the vicinity of the conserved-Hopf bifurcation.

This work is structured as follows. In Sec. II, we discuss the scaling properties resulting from the dispersion relation of the conserved-Hopf bifurcation and introduce the relatively simple but instructive example of a symmetric Cahn–Hilliard model with purely nonreciprocal linear coupling. We identify the resulting linear problem as a free-particle Schrödinger equation and discuss the resulting multi-scale ansatz in real and Fourier space. Subsequently, in Sec. III, we derive the leading-order amplitude equation and briefly discuss its structure and properties. In Sec. IV, we proceed by determining analytic solutions of the obtained amplitude equation, their linear stability, and the resulting bifurcation structure. The discussion carries over to Sec. V, where we quantitatively compare states, bifurcation structure, and time evolution obtained from the amplitude equation and from the symmetric purely nonreciprocally coupled fully nonlinear model. Finally, we lift the restrictions imposed by the simplicity of the case considered

in Secs. II–V and extend the developed approach toward the generic case. We summarize and conclude in Sec. VII.

II. SCALING, ANSATZ, AND SYMMETRY

We consider a system of spatially and temporally homogeneous and parity symmetric kinetic equations of first order in time for scalar fields. For simplicity, we consider a large, one-dimensional domain of size l with periodic boundary conditions. The Taylor-expanded dispersion relation for a conserved-Hopf bifurcation is[16]

$$\lambda_{\pm}(k) = \Delta(k) \pm i\Omega(k),$$

$$\Delta(k) = \mu k^2 - \delta' k^4 + \mathcal{O}(k^6), \qquad (1)$$

$$\Omega(k) = \omega k^2 - \omega' k^4 + \mathcal{O}(k^6),$$

where $\mu = \varepsilon^2 \tilde{\mu} \ll 1$, $\tilde{\mu} = \mathcal{O}(1)$, and $\omega = \mathcal{O}(1)$. In other words, the system is close to the onset of a conserved, large-scale, oscillatory instability, where for $\tilde{\mu} > 0$ modes with complex conjugate pairs of eigenvalues with $k < k_c = \varepsilon\sqrt{\tilde{\mu}/\delta'}$ will exponentially grow whereas all other modes will decay exponentially (see Fig. 1). A simple example, that, similar to the Swift–Hohenberg model for the Turing instability, directly and without Taylor-expansion yields the dispersion relation (1) is the symmetric Cahn–Hilliard model with purely nonreciprocal linear coupling,

$$\partial_t u = \partial_{xx}(-\mu u + u^3 - \partial_{xx}u - \omega v),$$

$$\partial_t v = \partial_{xx}(-\mu v + v^3 - \partial_{xx}v + \omega u), \qquad (2)$$

$$\text{in the particular case,} \quad \int_0^l u\,dx = \int_0^l v\,dx = 0.$$

This is a special case of the models analyzed in Refs. 30–35 and 40, where sometimes noise is added. Further simplified versions are obtained by linearizing the second equation.[38,39,41,42] Using a vector notation $\boldsymbol{u} = (u, v)$ and employing the usual ansatz $\boldsymbol{u}(t) = \boldsymbol{u}_0 + \delta\boldsymbol{u}(t)$ with $\delta\boldsymbol{u}(t) \sim \varepsilon\, e^{ikx - \lambda t} \ll 1$ in (2), i.e., adding a small perturbation $\delta\boldsymbol{u}$ to the trivial solution $u(x, t) = v(x, t) = 0$, we obtain the dispersion relation (1) with $\delta' = 1$ and $\omega' = 0$.
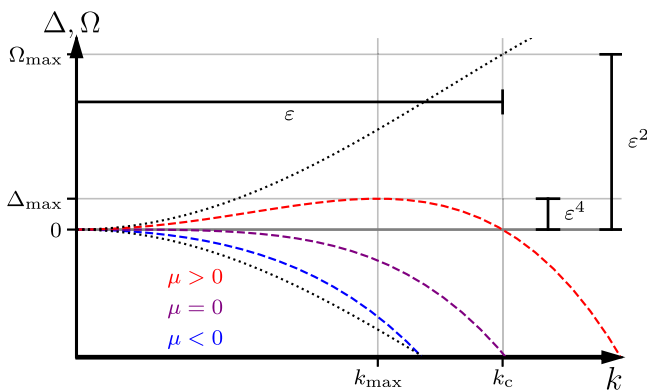
FIG. 1. Dispersion relation of the conserved-Hopf instability. The growth rate Δ is, respectively, shown in blue, purple, and red below ($\mu < 0$), at ($\mu = 0$) and above ($\mu > 0$) the onset of instability. The dotted lines indicate the corresponding frequencies $\pm\Omega$.

Next, we observe that the fastest growing wavenumber k_{max} is of $\mathcal{O}(\varepsilon)$, which implies that the dynamics occurs on the length scale $X = \varepsilon x$. This implies that the leading order oscillation in (1) occurs on the timescale $\tau = \varepsilon^2 t$, whereas the first contribution of the growth rates occurs on the timescale $T = \varepsilon^4 t$.

Note that one could similarly argue for the frequency $\Omega(k_{max})$ at the largest growing wavenumber k_{max} to be used for the fast timescale. However, since $k_{max} = k_c/\sqrt{2}$, this does not affect the scaling in ε. Then, we perform a weakly nonlinear analysis for the symmetric model (2) with the scalings $\partial_x = \varepsilon\partial_X$ and $\partial_t = \varepsilon^2\partial_\tau + \varepsilon^4\partial_T$ and

$$\boldsymbol{u}(t) = \varepsilon\boldsymbol{u}_1(X, \tau, T) + \varepsilon^2\boldsymbol{u}_2(X, \tau, T) + \varepsilon^3\boldsymbol{u}_3(X, \tau, T) + \text{h.o.t.} \quad (3)$$

The first nonvanishing contribution occurs at $\mathcal{O}(\varepsilon^3)$ and yields the homogeneous linear problem

$$\underline{\boldsymbol{L}}\boldsymbol{u}_1 = 0,$$

$$\text{with} \quad \underline{\boldsymbol{L}} = \underline{\boldsymbol{1}}\partial_\tau - \begin{pmatrix} 0 & -\omega \\ \omega & 0 \end{pmatrix}\partial_{XX}. \qquad (4)$$

This corresponds, up to prefactors, to the linear, i.e., free-particle Schrödinger equation.[43] Its general solution is

$$\boldsymbol{u}_1(X, \tau, T) = e^{i\omega\tau\partial_{XX}}A(X, T)\boldsymbol{e}_+ + e^{-i\omega\tau\partial_{XX}}A^*(X, T)\boldsymbol{e}_-, \qquad (5)$$

where $\boldsymbol{e}_\pm = (\pm i, 1)/\sqrt{2}$ (i.e., $\boldsymbol{e}_+ \perp \boldsymbol{e}_-$). In other words, $e^{i\omega\tau\partial_{XX}}$ corresponds to a time evolution operator, where $-\omega\partial_{XX}$ is the free-particle Hamiltonian and the slowly varying amplitude $A(X, T)$ takes to role of the initial wavefunction that (on the fast timescale τ) freely propagates in space. Note that the ansatz breaks down if $\omega = 0$ or $\omega = \mathcal{O}(\varepsilon^2)$, as then Eq. (4) becomes trivial ($\partial_\tau\boldsymbol{u}_1 = 0$) and all terms enter the expansion at $\mathcal{O}(\varepsilon^5)$, i.e., no separation of timescales is possible. This occurs, e.g., when studying the codimension-two point where a transition between Cahn–Hilliard instability and conserved-Hopf instability occurs. There, $\omega \to 0$ and the critical wave number is zero for both instabilities. Therefore, considering such a transition, the nonreciprocal Cahn–Hilliard (NRCH) model cannot be reduced by scale separation and, therefore, emerges as its own amplitude equation (see Ref. 16).

Next, we discuss the consequences of the ansatz (5) that arises from the linear problem at leading order. In general, the underlying symmetry of the original system, i.e., parity symmetry and homogeneity in space and time combined with the relation between amplitude and original variables implies consequences for the form of occurring nonlinearities. For instance, for the standard Hopf instability without conservation law, the usual ansatz is $\boldsymbol{u}(x, t) = \varepsilon\, e^{i\omega t}A(X, \tau)\boldsymbol{e}_+ + c.c.$ Then, homogeneity in time implies that the equations are invariant under the shift $t \to t + t_0$. Hence, on the amplitude level, amplitude A picks up a global phase $A(X, \tau) \to e^{i\omega t_0}A(X, \tau)$. From this, we can conclude that the simplest occurring nonlinearity is $\sim A|A|^2$ as it transforms like the linear term, i.e., $A|A|^2 \to e^{i\omega t_0}A|A|^2$, whereas quadratic or other cubic terms are forbidden, because, e.g., $A^2 \to e^{2i\omega t_0}A^2$ shows a different transformation behavior. (Analogously, for Turing instabilities, where $\boldsymbol{u}(x, t) = \varepsilon\, e^{ikx}A(X, \tau)\boldsymbol{e}_+ + c.c.$, the combination of homogeneity in space with additional parity invariance yields that the simplest nonlinearity is $\sim A|A|^2$ with a real coefficient.)

05 December 2024 16:45:27

We transfer this argument to the ansatz (5) for the conserved-Hopf instability. Here and in the following, it is instructive to discuss the problem in terms of Fourier modes, i.e., we introduce the usual Fourier transform $\tilde{A}(K, T)$, which fulfills $A(X, T) = \sum_K \tilde{A}(K, T)\, e^{iKX}$, where $K = 2\pi z/L$, with $L = \varepsilon l$ and $z \in \mathbb{Z}$. Hence, the amplitude transforms under $\tau \to \tau + \tau_0$ as

$$A(X, T) \to e^{i\omega\tau_0 \partial_{XX}} A(X, T)$$
$$= e^{i\omega\tau_0 \partial_{XX}} \sum_K \tilde{A}(K, T)\, e^{iKX}$$
$$= \sum_K e^{-i\omega\tau_0 K^2} \tilde{A}(K, T)\, e^{iKX}. \tag{6}$$

In other words, by the convolution theorem each Fourier mode $\tilde{A}(K, T)$ of the amplitude transforms individually as $\tilde{A}(K, T) \to e^{-i\omega\tau_0 K^2} \tilde{A}(K, T)$. This has dramatic consequences for nonlinearities of the amplitude equation. In particular, it rules out all local nonlinearities, as they generically couple distinct Fourier modes with nonuniform transformation behavior. However, (nonlocal) nonlinearities compatible with the symmetry can be explicitly constructed based on their Fourier space representation, like, e.g., $\mathcal{F}^{-1}[\tilde{A}|\tilde{A}|^2]$. Next, we will derive the amplitude equation, i.e., a dynamical equation for $A(X, T)$ at leading order.

III. LEADING ORDER AMPLITUDE EQUATION: SIMPLE CASE

At $\mathcal{O}(\varepsilon^4)$, we obtain a similar homogeneous linear system for $\boldsymbol{u}_2$ as Eq. (4) for $\boldsymbol{u}_1$ at $\mathcal{O}(\varepsilon^3)$. Here, it is not considered further as it does not contribute at $\mathcal{O}(\varepsilon^5)$. At $\mathcal{O}(\varepsilon^5)$, we obtain the inhomogeneous linear system

$$\underline{L}\boldsymbol{u}_3 = \boldsymbol{q}_5,$$
$$\text{with } \boldsymbol{q}_5 = \partial_{XX} \begin{pmatrix} -\tilde{\mu}u_1 + u_1^3 - \partial_{XX}u_1 \\ -\tilde{\mu}v_1 + v_1^3 - \partial_{XX}v_1 \end{pmatrix} - \begin{pmatrix} \partial_T u_1 \\ \partial_T v_1 \end{pmatrix}. \tag{7}$$

To apply a Fredholm alternative, we define a "spatiotemporal scalar product" in the function space of spatially L-periodic and temporally $1/\Omega$-periodic functions

$$\langle \boldsymbol{F}; \boldsymbol{G} \rangle = \frac{\Omega_{\min}}{L} \int_0^L dX \int_0^{1/\Omega_{\min}} d\tau\, \boldsymbol{F}^\dagger \boldsymbol{G}, \tag{8}$$

where $\Omega_{\min} = \omega K_{\min}^2/(2\pi) = 2\pi\omega/L^2$. Then, the integral of a harmonic function is only nonzero, i.e., $\frac{\Omega_{\min}}{L} \int_0^L dX \int_0^{1/\Omega_{\min}} d\tau\, e^{iKX} e^{i\Omega\tau} = 1$ if both spatial and temporal frequencies vanish ($K = \Omega = 0$). It is zero otherwise.

By the Fredholm alternative, Eq. (7) only has a solution if $\boldsymbol{q}_5$ is orthogonal to the kernel of the adjoint linear operator $\underline{L}^\dagger$, given by

$$\underline{L}^\dagger = -\underline{\mathbf{1}}\partial_\tau - \begin{pmatrix} 0 & \omega \\ -\omega & 0 \end{pmatrix} \partial_{XX} = -\underline{L}. \tag{9}$$

In line with Eqs. (4) and (5) at $\mathcal{O}(\varepsilon^3)$, the kernel of this linear operator is given by

$$\boldsymbol{m} = e^{i\omega\tau\partial_{XX}} B(X)\boldsymbol{e}_+ + e^{-i\omega\tau\partial_{XX}} C(X)\boldsymbol{e}_-, \tag{10}$$

where $B(X)$ and $C(X)$ are arbitrary functions. To obtain an equation for the amplitude $A(\hat{X}, T)$ we choose $B(X) = \delta(X - \hat{X})$ and $C(X) = 0$.[44] Then, applying the Fredholm alternative for the linear contributions in $\boldsymbol{q}_5$, i.e., evaluating their scalar product (8) with Eq. (10) and substituting $\boldsymbol{u}_1$ with the amplitude (5), we obtain

$$\langle \boldsymbol{m}; (-\tilde{\mu}\partial_{XX} - \partial_{XXXX} - \partial_T)\boldsymbol{u}_1 \rangle$$
$$= \langle e^{i\omega\tau\partial_{XX}} \delta(X - \hat{X})\boldsymbol{e}_+; (-\tilde{\mu}\partial_{XX} - \partial_{XXXX} - \partial_T)$$
$$\times (e^{i\omega\tau\partial_{XX}} A(X, T)\boldsymbol{e}_+ + e^{-i\omega\tau\partial_{XX}} A^*(X, T)\boldsymbol{e}_-) \rangle$$
$$= (-\tilde{\mu}\partial_{\hat{X}\hat{X}} - \partial_{\hat{X}\hat{X}\hat{X}\hat{X}} - \partial_T)A(\hat{X}, T), \tag{11}$$

where we employed the orthogonality of $\boldsymbol{e}_+$ and $\boldsymbol{e}_-$, and used the unitarity of the operator $e^{-i\omega\tau\partial_{XX}}$.[45] Next, we consider the cubic nonlinearities within $\boldsymbol{q}_5$. Inserting the amplitude $A(X, T)$ from (5) yields

$$\partial_{XX} \begin{pmatrix} u_1^3 \\ v_1^3 \end{pmatrix} = \partial_{XX} \Big[\left(e^{i\omega\tau\partial_{XX}} A(X, T)\right)^3 \boldsymbol{w}^{(1)}$$
$$+ 3\left(e^{-i\omega\tau\partial_{XX}} A^*(X, T)\right)\left(e^{i\omega\tau\partial_{XX}} A(X, T)\right)^2 \boldsymbol{w}^{(2)}$$
$$+ 3\left(e^{-i\omega\tau\partial_{XX}} A^*(X, T)\right)^2 \left(e^{i\omega\tau\partial_{XX}} A(X, T)\right) \boldsymbol{w}^{(3)}$$
$$+ \left(e^{-i\omega\tau\partial_{XX}} A^*(X, T)\right)^3 \boldsymbol{w}^{(4)} \Big]. \tag{12}$$

The $\boldsymbol{w}^{(i)}$ are given by

$$\boldsymbol{w}^{(1)} = \begin{pmatrix} (\boldsymbol{e}_+)_1^3 \\ (\boldsymbol{e}_+)_2^3 \end{pmatrix}, \quad \boldsymbol{w}^{(2)} = \begin{pmatrix} (\boldsymbol{e}_+)_1^2(\boldsymbol{e}_-)_1 \\ (\boldsymbol{e}_+)_2^2(\boldsymbol{e}_-)_2 \end{pmatrix},$$
$$\boldsymbol{w}^{(3)} = \begin{pmatrix} (\boldsymbol{e}_+)_1(\boldsymbol{e}_-)_1^2 \\ (\boldsymbol{e}_+)_2(\boldsymbol{e}_-)_2^2 \end{pmatrix} \quad \text{and} \quad \boldsymbol{w}^{(4)} = \begin{pmatrix} (\boldsymbol{e}_-)_1^3 \\ (\boldsymbol{e}_-)_2^3 \end{pmatrix}, \tag{13}$$

where $(\boldsymbol{e}_\pm)_1$ and $(\boldsymbol{e}_\pm)_2$ refer to the first and second component of $\boldsymbol{e}_\pm$, respectively. For the presently considered simple nongeneric choice of linear and nonlinear terms, we obtain $\boldsymbol{w}^{(1)} = \boldsymbol{w}^{(3)} = \boldsymbol{e}_-/2$ and $\boldsymbol{w}^{(2)} = \boldsymbol{w}^{(4)} = \boldsymbol{e}_+/2$.

First, we deal with the second term $\sim \boldsymbol{w}^{(2)}$ in (12), as it results in the dominant nonlinear contribution. We use the identity $\delta(X - \hat{X}) = \sum_Q e^{iQ(X-\hat{X})}$ and again express all occurring amplitudes by their Fourier transform $A(X, T) = \sum_K \tilde{A}(K, T)\, e^{iKX}$ to evaluate the scalar product,

$$3\left\langle e^{i\omega\tau\partial_{XX}} \delta(X - \hat{X})\boldsymbol{e}_+; \partial_{XX} \left(e^{-i\omega\tau\partial_{XX}} A^*(X, T)\right)\left(e^{i\omega\tau\partial_{XX}} A(X, T)\right)^2 \boldsymbol{w}^{(2)} \right\rangle$$

$$= \frac{3}{2} \left\langle e^{i\omega\tau\partial_{XX}} \sum_Q e^{iQ(X-\hat{X})}\boldsymbol{e}_+; \partial_{XX} \left(e^{-i\omega\tau\partial_{XX}} \sum_K \tilde{A}^*(K, T)\, e^{iKX}\right)\left(e^{-i\omega\tau\partial_{XX}} \sum_K \tilde{A}(K, T)\, e^{iKX}\right)^2 \boldsymbol{e}_+ \right\rangle$$

$$= \frac{3\Omega_{\min}}{2L} \sum_{Q,K,K',K''} e^{iQ\hat{X}} \tilde{A}^*(K,T)\tilde{A}(K',T)\tilde{A}(K'',T)(-Q^2) \int_0^{1/\Omega_{\min}} e^{i\omega\tau(Q^2+K^2-K'^2-K''^2)}\,d\tau \int_0^L e^{iX(-Q-K+K'+K'')}\,dX$$

$$= \frac{3}{2}\left[2\sum_Q e^{iQ\hat{X}}(-Q^2)\tilde{A}(Q,T)\sum_K \tilde{A}^*(K,T)\tilde{A}(K,T) - \sum_Q e^{iQ\hat{X}}(-Q^2)\tilde{A}(Q,T)\tilde{A}(Q,T)\tilde{A}^*(Q,T) \right]$$

$$= \frac{3}{2}\partial_{\hat{X}\hat{X}}\left(2\mathcal{F}^{-1}[\tilde{A}(K,T)\sum_{K'}|\tilde{A}(K',T)|^2] - \mathcal{F}^{-1}[\tilde{A}(K,T)|\tilde{A}(K,T)|^2] \right). \tag{14}$$

Here, the key observation is that the two integrals in the third line are zero, whenever one of the integrands has a nonzero phase. Therefore, only terms with

$$Q^2 + K^2 = K'^2 + K''^2 \quad \text{and} \quad Q + K = K' + K'' \tag{15}$$

contribute. Equations (15) has a strong analogy to an elastic collision, i.e., they correspond to the nonrelativistic, elastic $2 \to 2$ scattering of particles with equal mass, incoming momenta Q, K and outgoing momenta K', K''. In one dimension, the only possibilities are that the two particles exchange momenta or pass unhindered, i.e., the momenta are pairwise equal $Q = K'$ and $K = K''$ or $Q = K''$ and $K = K'$. After inserting into Eq. (14), both options yield the same contribution. However, if $Q = K$, the two solutions are identical, i.e., we have to account for overcounting, which is done by the second term in the fourth row of Eq. (14). Due to Parseval's identity, the first term transforms into real space, as $\mathcal{F}^{-1}[\tilde{A}(K,T)\sum_{K'}|\tilde{A}(K',T)|^2]$ $= A(X,T)\langle|A(X,T)|^2\rangle$, i.e., as a coupling to the mean of the squared amplitude. In real space, the second term can be expressed as the double-convolution $\mathcal{F}^{-1}[\tilde{A}|\tilde{A}|^2](X) = [A(\tilde{X}) \star A(\tilde{X}) \star A^*(-\tilde{X})](X)$, but we will keep the first notation for brevity. A similar consideration for the three remaining nonlinearities yields that they correspond to elastic $4 \to 0$, $3 \to 1$, and $1 \to 3$ scatterings of particles with equal mass in one dimension. Here, elastic means that energy and momentum are both conserved. However, mass is not conserved, e.g., for the $1 \to 3$ case, one particle splits into three particles, where each has identical mass as the incident particle. Trivial solutions, where some of the momenta equal zero do not contribute, since $A(K = 0, T) = 0$, which results from the mass conservation of the underlying system. Further, the latter two contributions are also negligible compared to the $2 \to 2$ scattering if the amplitude is sufficiently localized in Fourier space, which we assume. Finally, collecting all terms and reintroducing the original scales, i.e., introducing $a = \varepsilon A$, we obtain the amplitude equation

$$\partial_t a = \partial_{xx}\left(-\mu a + \frac{3}{2}(2a\langle|a|^2\rangle - \mathcal{F}^{-1}[\tilde{a}|\tilde{a}|^2]) - \partial_{xx} a \right), \tag{16}$$

where the coefficient(s) are all real. The nature of the nonlocal terms can be understood in terms of the dynamics on the different timescales: due to the dispersion relation $\Omega(k) \sim \pm\omega k^2$, each individual harmonic mode propagates with a distinct velocity $\pm\omega k$ on the fast timescale τ. As the propagation of the wave is very fast as compared to the growth of their amplitudes, during a characteristic time interval of amplitude growth, several wavelengths

of other waves will have passed, resulting in a nonlocal interaction. In other words, each wave interacts with the (squared) mean of all other waves. This holds for all interactions besides the self-interaction of a wave, since in this case the propagation velocity trivially coincides. The amplitude equation is related to the dynamics of the original fields u via

$$u(x,t) = e^{i\omega t\partial_{xx}} a(x,t)e_+ + e^{-i\omega t\partial_{xx}} a^*(x,t)e_-. \tag{17}$$

The dispersion relation of Eq. (16) is $\lambda(k^2) = \mu k^2 - k^4$, i.e., compared to the general Eq. (1), the frequencies $\pm\omega k^2$ on the fast timescale do no longer appear, i.e., the fast timescale has been fully separated. In the considered case, the instability is even stationary, i.e., the eigenvalues $\lambda(k^2)$ are all real. However, this is a nongeneric consequence of our minimal choice (2), i.e., without a contribution $\sim k^4$ to the frequency, i.e., $\omega' = 0$ in Eq. (1). The general case is treated below in Sec. VI.

Remarkably, the obtained amplitude equation with real coefficients has the structure of a gradient dynamics for a conserved complex field, i.e., it can be written in the form

$$\partial_t a = \partial_{xx}\frac{\delta\mathcal{G}[a]}{\delta a^*}, \tag{18}$$

where the underlying energy functional is

$$\mathcal{G}[a] = \int_{-l/2}^{l/2}\left(-\mu|a|^2 + |\partial_x a|^2 \right)dx + \frac{3l}{2}\left(\frac{1}{l}\int_{-l/2}^{l/2}|a|^2\,dx \right)^2$$
$$- \frac{3}{4l^2}\iiint_{[-\frac{l}{2},\frac{l}{2}]^3} a^*(x)a^*(-x')a(x'')a(x-x'-x'')\,dx\,dx'\,dx''. \tag{19}$$

The energy is more intuitively understood, if it is expressed by the Fourier amplitude $\tilde{a}$, where $a(x,t) = \sum_k \tilde{a}(k,t)e^{ikx}$. It reads

$$\mathcal{G}[\tilde{a}] = l\sum_k\left[(-\mu + k^2)|\tilde{a}|^2 - \frac{3}{4}|\tilde{a}|^4 \right] + \frac{3l}{2}\left(\sum_k |\tilde{a}|^2 \right)^2. \tag{20}$$

As $\left(\sum_k |\tilde{a}|^2\right)^2 \geq \sum_k |\tilde{a}|^4$, for large values of $\tilde{a}$, the energy is dominated by the strictly positive last term. This shows that it is bounded

from below. The variational character of (18) has important impli-
cations: The evaluation of the total time derivative of $\mathcal{G}[a]$, i.e.,

$$
\begin{aligned}
\frac{\mathrm{d}}{\mathrm{d}t}\mathcal{G}[a] &= \int_{-l/2}^{l/2} \left(\frac{\delta\mathcal{G}}{\delta a^*}\frac{\mathrm{d}a^*}{\mathrm{d}t} + \frac{\delta\mathcal{G}}{\delta a}\frac{\mathrm{d}a}{\mathrm{d}t} \right) \mathrm{d}x \\
&= \int_{-l/2}^{l/2} \left[\frac{\delta\mathcal{G}}{\delta a^*}\left(\partial_{xx}\frac{\delta\mathcal{G}}{\delta a}\right) + \frac{\delta\mathcal{G}}{\delta a}\left(\partial_{xx}\frac{\delta\mathcal{G}}{\delta a^*}\right) \right] \mathrm{d}x \\
&\overset{\text{p.I.}}{=} -2\int_{-l/2}^{l/2} \left| \partial_x\frac{\delta\mathcal{G}}{\delta a} \right|^2 \mathrm{d}x \le 0
\end{aligned}
\tag{21}
$$

demonstrates that $\mathcal{G}[a]$ is a Lyapunov functional. This implies that
the amplitude $a(x,t)$ will always eventually approach a stable steady
state, and all stable steady states will only show eigenmodes with real
eigenvalues. That is, no oscillatory dynamics occurs on the level of
the amplitude equation, although it does on the level of the original
fast dynamics.

Next, we will analyze the analytical solutions of the amplitude
equation (16) and relate them to the dynamics of the full model.

IV. STATES AND THEIR STABILITY

Before entering fine details, we discuss the simple harmonic
solution to the amplitude equation (16). As shown below, it is
given by

$$
a(x,t) = a_0\,e^{iqx}, \quad \text{with} \quad |a_0|^2 = \frac{2}{3}(\mu - q^2),
\tag{22}
$$

where $|q| \in (0,\sqrt{\mu})$ for $\mu > 0$. Using Eq. (17) to translate this back
into the original fields, i.e., applying the linear Schrödinger-like time
evolution yields

$$
\boldsymbol{u} = \sqrt{2}|a_0| \begin{pmatrix} \sin\left(qx + \omega q^2 t + \phi\right) \\ \cos\left(qx + \omega q^2 t + \phi\right) \end{pmatrix}.
\tag{23}
$$

Therefore, a single-mode harmonic solution of the amplitude
equation corresponds to a traveling wave with velocity $-\omega q$, where
the fields u_1 and u_2 are phase shifted by $\pi/2$. Left-traveling (right-
traveling) waves are, hence, given by $q > 0$ ($q < 0$). The global phase
ϕ is undetermined and reflects translational symmetry.

To find the general solution of the steady state equation, i.e.,
Eq. (16) with $\partial_t a = 0$, we integrate twice. The first integration con-
stant is zero as we request the net flux to be zero. Remarkably, here
we can also eliminate the second integration constant as we have to
request $\bar{a} = 0$, because the amplitude a defines the perturbation with
respect to the mean value of the original field. As a result, we have

$$
-\mu a + 3a\langle|a|^2\rangle - \frac{3}{2}\mathcal{F}^{-1}[\tilde{a}|\tilde{a}|^2] - \partial_{xx}a = 0.
\tag{24}
$$

To solve it, we reintroduce the Fourier transform, i.e., we substitute
$a(x,t) = \sum_q \tilde{a}(q)\,e^{iqx}$ to obtain

$$
\sum_q \left(-\mu + 3\sum_k |\tilde{a}(k)|^2 - \frac{3}{2}|\tilde{a}(q)|^2 + q^2 \right) \tilde{a}(q)\,e^{iqx} = 0.
\tag{25}
$$

Since the e^{iqx} are linearly independent, all contributing modes,
i.e., all modes where $\tilde{a}(q) \ne 0$ satisfy $-\mu + 3\sum_k |\tilde{a}(k)|^2 - \frac{3}{2}|\tilde{a}(q)|^2$
$+ q^2 = 0$. We can, therefore, construct solutions as follows: We

pick an arbitrary set of N pairwise distinct contributing modes
$q_1, \ldots, q_N$. Then, the mean squares of their amplitudes $\tilde{a}_1, \ldots, \tilde{a}_N$
are determined by the linear system

$$
\begin{pmatrix} \frac{1}{2} & 1 & \cdots & 1 \\ 1 & \frac{1}{2} & \cdots & 1 \\ \cdots & \cdots & \cdots & \cdots \\ 1 & 1 & \cdots & \frac{1}{2} \end{pmatrix} \begin{pmatrix} |\tilde{a}_1|^2 \\ |\tilde{a}_2|^2 \\ \cdots \\ |\tilde{a}_N|^2 \end{pmatrix} = \frac{1}{3} \begin{pmatrix} \mu - q_1^2 \\ \mu - q_2^2 \\ \cdots \\ \mu - q_N^2 \end{pmatrix},
\tag{26}
$$

and the phases are left arbitrary. As the solutions have to fulfill
$|\tilde{a}_i|^2 > 0$ for all i, for each configuration, there exists a thresh-
old value μ_t, such that the solution exists if $\mu > \mu_t$. Note that
the single-mode solution arises as the special case for $N = 1$, i.e.,
$\frac{1}{2}|\tilde{a}_1|^2 = \frac{1}{3}(\mu - q_1^2)$. To illustrate the procedure and its result, we
also detail the case $N = 2$, where Eq. (26) reduces to

$$
\begin{pmatrix} \frac{1}{2} & 1 \\ 1 & \frac{1}{2} \end{pmatrix} \begin{pmatrix} |\tilde{a}_1|^2 \\ |\tilde{a}_2|^2 \end{pmatrix} = \frac{1}{3} \begin{pmatrix} \mu - q_1^2 \\ \mu - q_2^2 \end{pmatrix}
\tag{27}
$$

and is solved by

$$
\begin{pmatrix} |\tilde{a}_1|^2 \\ |\tilde{a}_2|^2 \end{pmatrix} = \frac{2}{9} \begin{pmatrix} \mu + q_1^2 - 2q_2^2 \\ \mu - 2q_1^2 + q_2^2 \end{pmatrix}.
\tag{28}
$$

For $q_1 = -q_2 =: q_s$, the two equations reduce to

$$
|\tilde{a}_{1,2}|^2 = \frac{2}{9}(\mu - q_s^2).
\tag{29}
$$

Notably, the condition for the existence of the solution is $\mu - q_s^2 > 0$
and is, therefore, the same as for the single harmonic mode with the
same wavelength. Specifically, if $\tilde{a}_1 = \tilde{a}_2$, the solution reads

$$
a(x,t) = \tilde{a}_s\cos(kx), \quad \text{with} \quad |\tilde{a}_s|^2 = \frac{8}{9}(\mu - q_s^2).
\tag{30}
$$

For this solution, the original fields become

$$
\boldsymbol{u}(x,t) = \sqrt{2}|\tilde{a}_s|\cos(kx) \begin{pmatrix} \sin(\omega q_s^2 t + \phi) \\ \cos(\omega q_s^2 t + \phi) \end{pmatrix},
\tag{31}
$$

which is a standing wave, where independently of space and time,
the two fields are phase-shifted in time by $\frac{\pi}{2}$. Note that this state
can be seen as a superposition of the left and right-traveling waves,
i.e., the already discussed single-mode states. For the case $q_2 > q_1$,
Eq. (28) has a solution, when $\mu - 2q_2^2 + q_1^2 > 0$, i.e., it only exists for
μ-values that are strictly larger than the critical ones for the individ-
ual modes with wavenumbers q_1 and q_2. Further, we note that any
(multi-mode) steady state of the amplitude equation corresponds to
a superposition of traveling waves in the full model. Here, we call
them oscillatory states. Figure 2 gives a schematic overview of the
discussed states on the two levels of description, i.e., the full dynamic
equation and the amplitude equation with real coefficient.

To analyze the stability of the single-mode states described
above, we introduce a small complex perturbation $\epsilon a_p(x,t)$ with
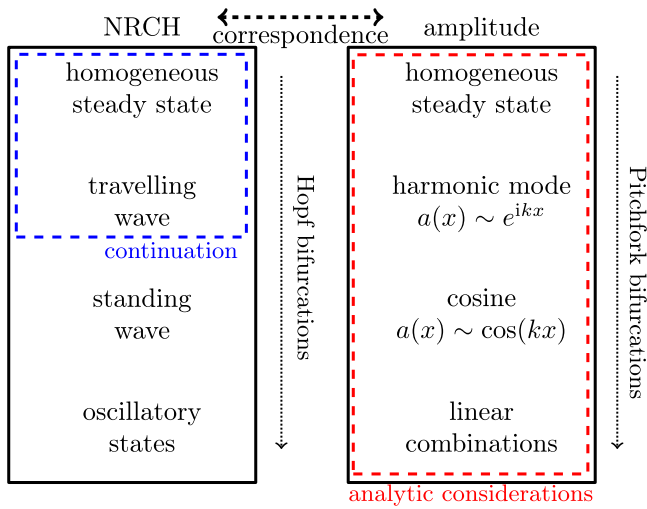
FIG. 2. Scheme of the corresponding states in the nonreciprocal Cahn–Hilliard (NRCH) model (2) and the obtained amplitude equation with real coefficients (16). The blue rectangle highlights the states captured with numerical path continuation, whereas the right rectangle displays states that are obtained from analytic considerations in Sec. IV.

$\epsilon \ll 1$,

$$a(x,t) = \sqrt{\frac{2}{3}(\mu - q^2)}\, e^{iqx} + \varepsilon a_p(x,t),$$ (32)

$$\text{with} \quad a_p(x,t) \sim e^{ikx + \lambda t}.$$

Inserting into (16) and linearizing in ϵ yields the dispersion relation

$$\lambda(k) = k^2 \left[-\delta_{k,q}(\mu - q^2) - \mu + 2q^2 - k^2 \right].$$ (33)

The discontinuity, i.e., the term $\sim \delta_{k,q}$ arises from the evaluation of integrals $\sim \int_0^l e^{i(k-q)x}\, dx$ that correspond to Fourier transforms of harmonics and are related to the second nonlinear term in Eq. (16), i.e., to the self-interaction of a traveling wave discussed in Sec. III. Examples of dispersion relations are given in Fig. 3.

For a specific q, the single-mode solution is stable if the square bracket in Eq. (33) is negative for all k. Since $\mu - q^2 > 0$ is necessary for the existence of the single-mode solution with wavelength

q, the discontinuity is always stabilizing. Therefore, Eq. (33) represents a large-scale instability if $-\mu + 2q^2 - k^2 > 0$ for some k. In a finite system of size l, the spectrum of wavenumbers is discrete, such that the first allowed perturbation occurs at $k = k_{\min} = 2\pi/l$ [see Fig. 3(c)]. In other words, q is linearly stable if

$$q^2 \le \frac{1}{2}\left(\mu + k_{\min}^2\right).$$ (34)

In the limit of an infinite system, i.e., for $k_{\min} \to 0$, the condition for linear stability reduces to

$$q^2 \le \frac{\mu}{2}.$$ (35)

This implies that for any sufficiently large domain, there exist several states with wavenumbers in the stable band, i.e., with $q \in [-\sqrt{\mu/2}, \sqrt{\mu/2}]$, i.e., we find a multistability of traveling waves of different wavelengths in the full system. This is in stark contrast to the amplitude equation for the stationary large-scale instability with conservation law, i.e., the Cahn–Hilliard equation, where the only stable state has a structure length of system size.

The multistability of traveling wave solutions naturally raises the question of wavelength selection, i.e., as there exist stable single-mode states of various different wavenumbers, it is an intriguing question, which state a system is likely to realize as a function of the initial condition. To investigate this question and further validate our findings, we continue with a numerical comparison of the dynamics as captured by the amplitude equation (16) and by the full model (2).

V. BIFURCATION ANALYSIS AND TIME SIMULATIONS

For the numerical analysis, we employ bifurcation techniques[46,47] and direct time simulations. Both are applied to the full dynamics (2) and the amplitude Eq. (16).

Remarkably, all steady states of the amplitude equation can be analytically determined as superpositions of (arbitrarily many) harmonics, as discussed in Sec. IV. As the NRCH dynamics contains various oscillatory states that are not easily tracked by numerical continuation, we restrict our attention to simple steady states and traveling waves. As solution measures, we employ the L^2-norms of
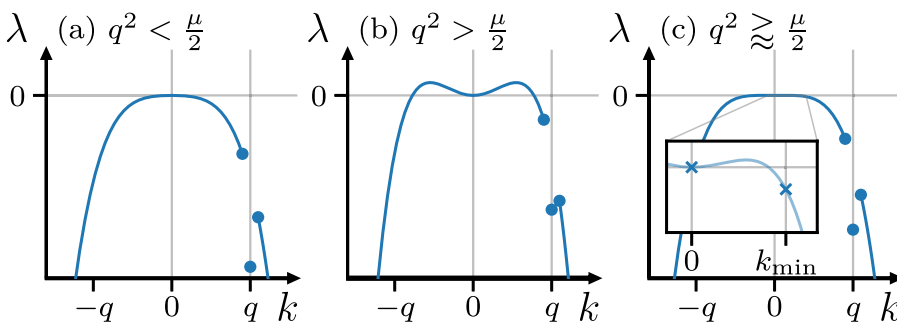
FIG. 3. Shown are selected dispersion relations of the single mode solution according to Eq. (33). Panels (a) and (b) show the stable and unstable case, respectively. Panel (c) illustrates the effect of the discretized wavenumbers on the linear stability, i.e., in the displayed dispersion relation the wavenumber q is unstable in the infinite-system limit but stable for a finite domain of length $2\pi/k_{\min}$. The term $\sim \delta_{k,q}$ in Eq. (33) $q = k$ leads to a discontinuity at $k = q$, which is indicated by blue dots.

the amplitude and of the original fields, i.e.,

$$\|a\|_{L^2} = \left(\frac{2}{l} \int_{-l/2}^{l/2} |a|^2 \, \mathrm{d}x\right)^{\frac{1}{2}},$$

$$(36)$$

$$\|\boldsymbol{u}\|_{L^2} = \left(\frac{1}{l} \int_{-l/2}^{l/2} (u^2 + v^2) \, \mathrm{d}x\right)^{\frac{1}{2}},$$

respectively. To account for relation (17) between a and $\boldsymbol{u} = (u, v)$, the norm of a is scaled by a factor $\sqrt{2}$, such that the single-mode solution of the amplitude equation and the corresponding traveling wave in the full dynamics have the same norm. The numerical continuation of the NRCH dynamics is performed employing the finite-element library *pde2path*.[48]

For the time simulations, we use a pseudo-spectral, semi-implicit Euler method for both the amplitude equation and the full dynamics, where the time-step is adapted via a half-step method. To allow for a comparison we match the initial condition by projecting $\boldsymbol{u}(x, t = 0)$ onto the initial amplitude $a(x, t = 0)$, apply the respective nonlinear time-evolution on the two levels of description and then calculate the approximated solution from the amplitude equation $u_a(x, t)$ using the linear Schrödinger relation (17).

We start with a discussion of the bifurcation structure. Figure 4(a) collects the analytical considerations from Sec. IV in a bifurcation diagram whereas Fig. 4(b) presents the homogeneous steady state and traveling wave states of the full model as obtained by path continuation. In Fig. 4(a), at $\mu = 0.01$, the homogeneous state becomes unstable with respect to the system-spanning mode with $k_{\min} = \frac{2\pi}{l}$ in a pitchfork bifurcation. Beyond the bifurcation, the homogeneous state has a fourfold degenerate positive eigenvalue, corresponding to real and imaginary perturbations with $\pm k_{\min}$. Note that for a more transparent comparison with the real fields of the nonreciprocal Cahn-Hilliard equation, we count real degrees of freedom. Therefore, every eigenvalue of the complex equation is twice degenerate as any complex perturbation corresponds to an arbitrary linear combination of real and imaginary part. At the bifurcation, three branches emerge, corresponding to the linearly stable harmonic functions $a \sim e^{\pm i k_{\min}x}$ and their unstable superposition $a \sim \cos(k_{\min}x)$. Note that the former two have identical norms as they are related by symmetry.

Similar bifurcations occur on the homogeneous steady state branch (primary branch) for all modes with $k_n = n k_{\min}$, in Fig. 4 shown up to $n = 6$, each further destabilizing the trivial state (with fourfold degeneracy). Next, following the secondary ($n = 2$)-branch, we observe another pitchfork bifurcation. At $\mu \approx 0.06$, three tertiary branches emerge from the secondary branch, corresponding to the linear combinations of two modes with wavenumbers $n = 1$ and $n = 2$. There, the fourfold degenerate eigenvalue changes its sign from positive to negative and the secondary ($n = 2$)-branch is stabilized. Something similar occurs for the secondary ($n = 3$)-branch that emerges from the primary branch with two fourfold degenerate positive eigenvalues. Following the branch, we see that first the two-mode solutions with $n = \{1, 3\}$ emerge stabilizing the first eigenvalue and second the two-mode solutions with $n = \{2, 3\}$ emerge, stabilizing also this secondary branch [see inset in Fig. 4(a)]. Similar successive stabilization occurs for every secondary
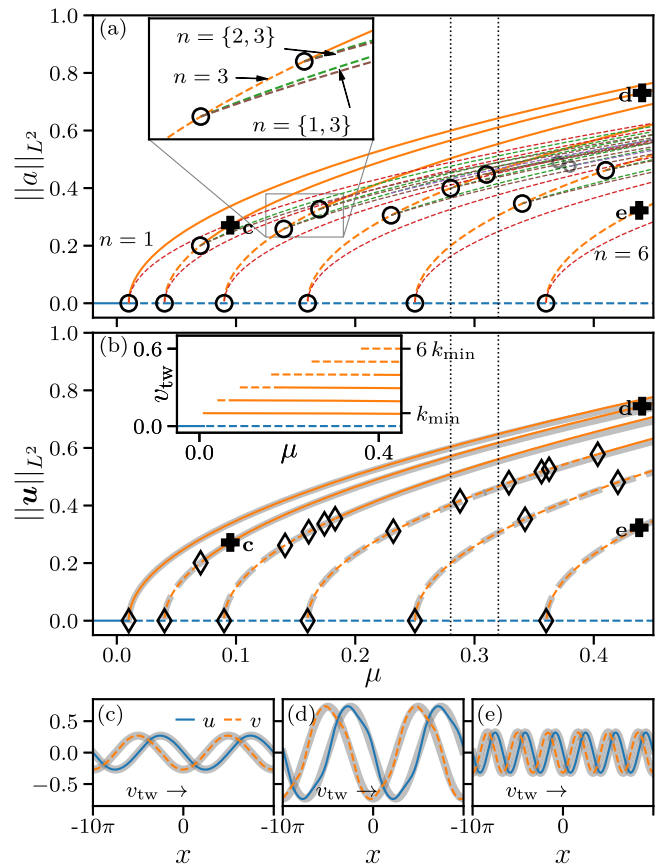

FIG. 4. Bifurcation diagrams obtained for (a) the amplitude equation (16) and (b) the symmetric NRCH model (2). Solid (dashed) lines represent stable (unstable) states. The light gray lines in (b) reproduce the single-mode branches from (a) to allow for direct comparison. The inset in panel (b) shows the velocity v_{tw} of traveling waves. Large circles and diamonds mark pitchfork and Hopf bifurcations, respectively, while the small circles indicate bifurcations on tertiary (two-mode) branches. Panel (a) additionally includes cosine modes (red), the superposition of harmonic modes with two (three) distinct wavenumbers [green (purple)] and superpositions of cosine and harmonic modes (brown). Panels (c), (d), and (e) show $\boldsymbol{u}$-profiles for the traveling wave states at loci marked by the crosses in (b), thereby the light gray curves reflect the real and imaginary part of the corresponding steady states in the amplitude equation (rescaled by a factor $\sqrt{2}$). The dotted vertical lines in (a) and (b) indicate the parameter values where the time simulations in Fig. 6 are performed. The domain size is $l = 20\pi$.

branch, i.e., the ($n = i$)-branch is stabilized via $i - 1$ consecutive pitchfork bifurcations.

Our analytic consideration allows us to find further branches—in fact, all branches—for example, those with three contributing modes, which emerge from the ones with two contributing modes in further bifurcations, indicated by the small circles in Fig. 4(a).

Next, turning to the bifurcation diagram of the corresponding NRCH system displayed in Fig. 4(b), we see that each pitchfork bifurcation of the trivial branch in Fig. 4(a) exactly corresponds to a Hopf bifurcation in Fig. 4(b). At each bifurcation, four complex
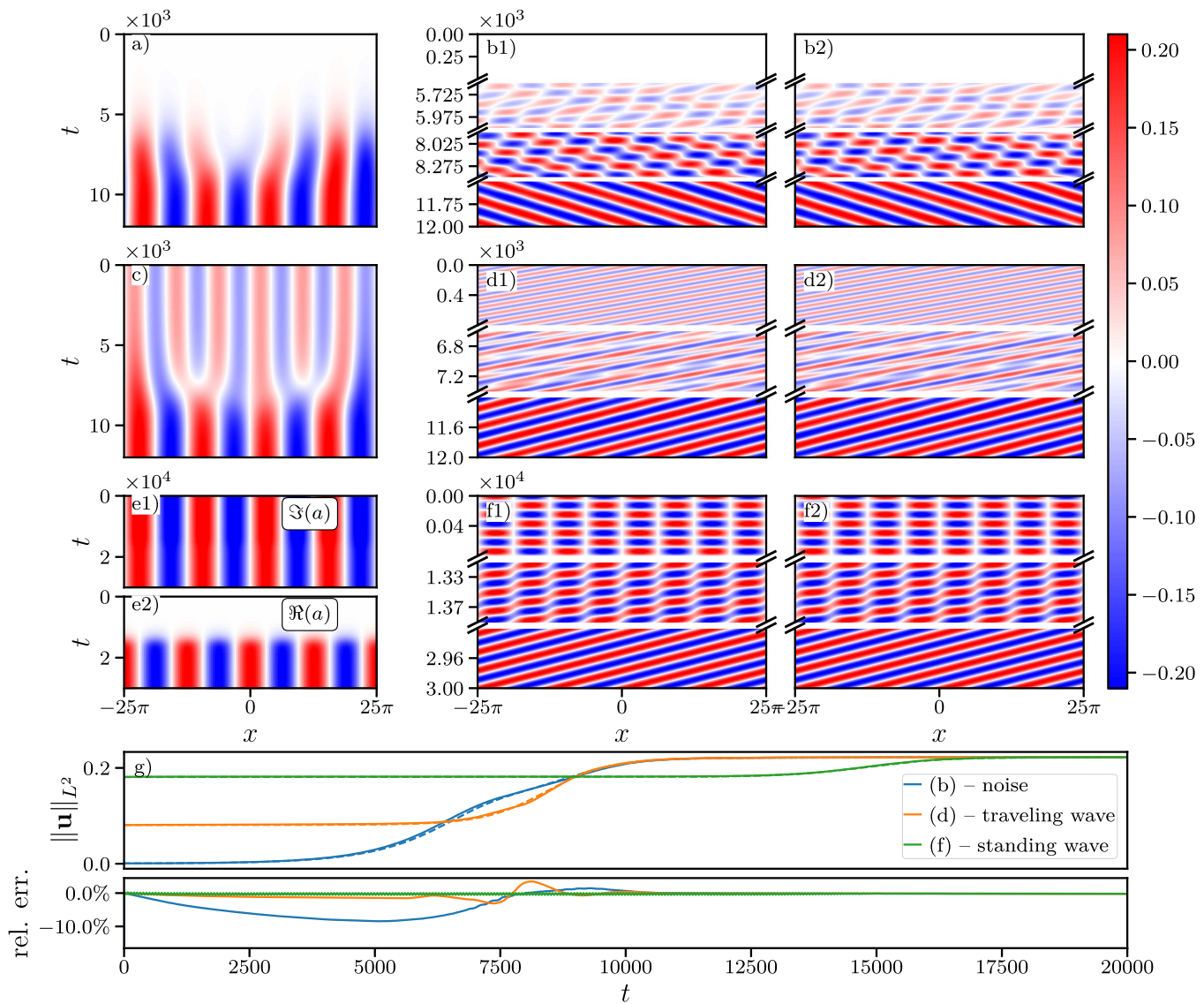
FIG. 5. Space–time plots for the amplitude (left column), the approximate dynamics for u_a reconstructed from the amplitude equation (middle column) and the full dynamics u obtained with the NRCH model (right column) with different initial condition, namely, white noise (first row), an unstable traveling wave (second row) and a standing wave (third row). Panels (a), (c), and (e1) show $\Im(a)$, whereas (e2) shows $\Re(a)$. Panels (b), (d), and (f) display u. Panel (g) shows the temporal evolution of the L^2-norm $\|u\|_{L^2}$ of the middle (right) column as dashed (solid) lines as well as their signed relative deviation. The parameters are $\mu = 1/16$, $\omega = 1$, and $l = 50\pi$. The spatial discretization consists of 512 points and the adapted timestep is usually around 1×10^{-2} for the full dynamics and 1×10^{-1} for the amplitude equation.

eigenvalues cross the imaginary axis, corresponding to two identical pairs of complex conjugate eigenvalues, one for the left- and one for the right-traveling wave. Despite our technical restriction to the continuation of traveling wave states, it is obvious that another branch will emerge that corresponds to standing wave states formed by the superposition of right- and left-traveling wave. In fact, the degeneracy is a general consequence of the translation- and parity invariance of the system, i.e., it is guaranteed by the underlying

O(2)-symmetry and can be rigorously proven as the *equivariant Hopf-theorem*.[49,50]

Following the emerging traveling wave branches, we see that, analogously to the amplitude equation, the $(n = 1)$-branch is unconditionally stable, whereas branches for higher n are at first unstable but stabilize in a sequence of Hopf bifurcations. With the exception of the $(n = 2)$-branch, where the numerical precision is not sufficient to unambiguously tell, the degeneracy is partly lost,

i.e., the ($n = 3$)-branch stabilizes in four consecutive Hopf bifurcations, where at each only one complex conjugate pair of eigenvalues crosses the imaginary axis. In the case of the amplitude equation, the degeneracy is due to the relative sign of the superposed harmonic mode having no impact, i.e., the superpositions of the contributing modes $\{k_2, k_1\}$ and $\{k_2, -k_1\}$ behave identically. In the case of the full dynamics, this would mean that the superposition of a right-traveling wave with a left-traveling wave behaves analogously to the superposition of a right-traveling wave with a right-traveling wave. As the corresponding degeneracy is not seen in the full dynamics, we speculate that it will also be lifted if the weakly nonlinear analysis is expanded up to a higher-order.

Figures 4(c)–4(e) show three examples of traveling wave states obtained by numerical continuation. The underlying gray lines show the steady states as obtained from the imaginary and real part of the corresponding solution of the amplitude equation, demonstrating that they also quantitatively match. Note that further away from the primary instability, the traveling waves are deformed, i.e., they do not have an exact harmonic shape as predicted by the amplitude equation. The inset of Fig. 4(b) shows that the velocity of

the traveling waves does not depend on the control parameter and scales linearly with the periodicity n. This quantitatively agrees with the dispersion relation that yields the traveling wave velocity $v_{tw} = \Omega(k_n)/k_n = \omega k_n$.

Next, we discuss time simulations performed close to the critical point, here at $\mu = 1/16$, to verify that the amplitude equation also correctly reflects the transient dynamics from an arbitrary initial condition toward a stable traveling wave. We chose the domain size $l = 50\pi$ in contrast to $l = 20\pi$ in Fig. 4, such that the previous analytical consideration predicts, that the ($n = 4$)-traveling wave is the stable solution with the largest wavenumber. Figures 5(a)–5(f) show space–time plots for various initial conditions, namely, (top) white noise, (center) an unstable ($n = 6$)-traveling wave solution and (bottom) an ($n = 4$)-standing wave solution. The latter two are superposed with white noise of small amplitude ($\sim 10^{-3}$). Panels (b1), (d1), and (f1) show the field u_a predicted from the amplitude equation, whereas panels (b2), (d2), and (f2) show the full dynamics of u. As we cannot visually resolve all oscillations over the whole simulation time, we show intermediate time intervals at critical times, i.e., when transitions occur. With the exception of (e),
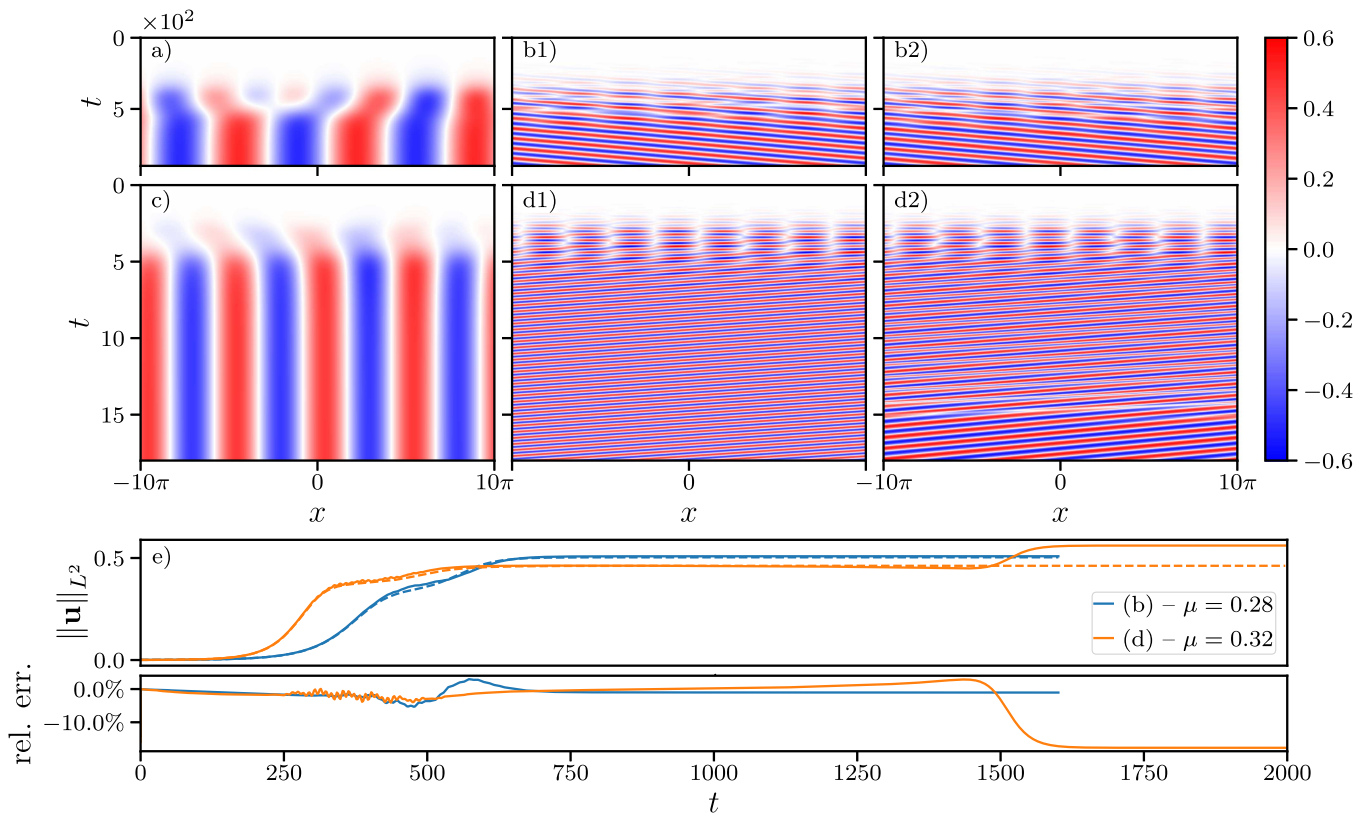
FIG. 6. Space–time plots for the amplitude Im(a) [panels (a) and (c)], the approximate dynamics for u_a obtained from the amplitude equation [panels (b1) and (d1)] and the full dynamics u of the NRCH model [panels (b2) and (d2)] with white noise initial condition ($\sim 10^{-3}$) at $\mu = 0.28$ (first row) and $\mu = 0.32$ (second row) and $l = 20\pi$. Panel (e) shows the temporal evolution of the L^2-norm $\|u\|_{L^2}$ of the middle (right)column as dashed (solid) lines as well as their signed relative deviation. The blue line that corresponds to panel (b) ends at $t = 1600$ as the numerical simulation has already converged to a stationary state. The spatial discretization consists of 512 points and the adapted timestep is usually around 8×10^{-4} for the full dynamics and 3×10^{-3} for the amplitude equation.

we only show Im(a) and u because Re(a) and v are qualitatively similar due to the underlying symmetries. For all initial conditions, the adapted timestep for the amplitude dynamics is persistently around one order of magnitude larger than for the full model, which roughly coincides with the ratio between fast and slow timescale of $\varepsilon^2 = \mu = 1/16$.

As u and u_a are visually indistinguishable in all panels, we conclude that the dynamics is well described by the amplitude equation, even after long simulation times. All the considered initial conditions settle to the ($n = 4$)-traveling wave state. Simulations with white noise are repeated 10 times (not shown) and always yield the same final state, with left- and right-traveling waves appearing approximately equally often. This indicates that the basin of attraction of the ($n = 4$)-solution is large compared to the one of the stable traveling wave states of lower periodicity. This is supported by the fact that it has the largest growth rate in the linear regime.

In the case of the unstable ($n = 6$)-traveling-wave in Figs. 5(c) and 5(d), one observes that it does not transition to an intermediate ($n = 5$)-state, but after nearly staying the same until $t \approx 5 \times 10^3$ directly transitions into the ($n = 4$)-state. The standing wave solution in panels (e) and (f) also remains nearly unchanged until at $t \approx 10^4$, it transitions into a traveling wave. As the standing wave initial condition here corresponds to a zero real part of the amplitude, real and imaginary parts show qualitatively different behaviors. The imaginary part stays unchanged and the real part grows until it reaches the same magnitude at $t \approx 1.5 \times 10^4$. As expected for a single-mode state, real and imaginary parts of the amplitude are phase shifted by $\pi/2$.

In Fig. 5(g), we compare the temporal evolution of the L^2-norm, Eq. (36) between the dynamics reconstructed from the amplitude equation and determined with the underlying NRCH model. The largest relative error $(\|u_a\|_{L^2} - \|u\|_{L^2})/\|u\|_{L^2}$ is smaller than 10% and occurs during the transition regime at $t \approx 5000$, whereas it almost vanishes for the final states. To conclude the discussion of the behavior close to the onset of the instability, we emphasize that time simulations have to be treated with special care when judging the stability of time periodic states. Despite being unstable, all intermediate states in panels (b), (d), and (f) of Fig. 5 stay qualitatively unchanged for many temporal periods, here up to 50 periods for the standing wave state. This is not unique to the conserved-Hopf bifurcation as any multiscale analysis aims to separate a slow transient at the onset of instability. However, here the linear Schrödinger-type relationship between fast and slow timescales causes intricate transient oscillations on the fast timescale. In contrast to this, in panels (a), (c), and (e) of Fig. 5, i.e., on the slow timescale, the dynamics looks surprisingly simple.

Finally, we briefly demonstrate that further away from the onset of the instability we start to see qualitative differences between the amplitude equation and the full dynamics. Following the previous discussion of the bifurcation analysis, we note in Fig. 4 that at $\mu = 0.28$ both models predict the ($n = 4$)-traveling wave state to be unstable. At $\mu = 0.32$ though, the amplitude equation predicts it to have stabilized, whereas the full model predicts it to be still unstable (see the dotted vertical lines in Fig. 4). The result of time simulations at these two μ-values with white noise initial conditions is displayed in Fig. 6. The observed final states are in all cases in line with the stability results of the respective bifurcation analysis.

Figures 6(a) and 6(b) at $\mu = 0.28$ retain the qualitative agreement between amplitude and full dynamics. Note that during the formation of the pattern, i.e., at $t \approx 350$ intermediate ($n = 4$)-structures appear that due to their instability later give way to the final ($n = 3$)-state. These ($n = 4$)-structures similarly appear in Figs. 6(c) and 6(d) at $\mu = 0.32$, with the difference that they are stable and represent the final state obtained with the amplitude equation, but not with the full model. Until $t \approx 500$, panels (d1) and (d2) look qualitatively similar. Although both then transition into an ($n = 4$)-traveling wave state, there the full dynamics in panel (d2) starts to show a modulation, i.e., individual peaks become thinner (wider) and higher (lower) with a higher period than the traveling wave, until at $t \approx 1500$ two peaks merge and the dynamics settles to a stable ($n = 3$)-traveling wave state. This is also visible in the temporal evolution of the L^2-norm in Fig. 6(e), as for both cases, the curves for reconstructed and full dynamics qualitatively agree until $t \approx 1500$. Consequently, the relative error is below 5% with the exception of the final state in (d), where the deviation is approximately 15%.

VI. LEADING ORDER AMPLITUDE EQUATION: GENERIC CASE

As shown in Ref. 16, a scalar (multi-field) model that features a conserved-Hopf instability, i.e., a large-scale oscillatory instability involving two conservation laws, can in the vicinity of the instability's onset always be reduced to a dynamical equation for two conserved scalar order parameter fields with nonlinearities up to third order in the fields. The NRCH model (2) we treated in Sec. III has an additional "odd" field-exchange symmetry $(u, v) \rightarrow (-v, u)$. In consequence, the resulting nonlocal amplitude equation (16) has a gradient dynamics structure that is not generic as will be shown next.

To treat the generic case, we break the mentioned field-exchange symmetry by considering the system

$$\partial_t u = \partial_{xx}(-\sigma_1 u + u^3 - \partial_{xx} u - (\rho + \alpha)v),$$
$$\partial_t v = \partial_{xx}(-\sigma_2 v + v^3 - \kappa \partial_{xx} v - (\rho - \alpha)u), \qquad (37)$$
$$\text{with} \quad \frac{1}{l} \int_0^l u\, dx = \bar{u} \quad \text{and} \quad \frac{1}{l} \int_0^l v\, dx = \bar{v}.$$

Note that we do not use the general system obtained in Ref. 16. Instead, to keep the calculations manageable, we only additionally introduce the rigidity ratio κ and a reciprocal linear coupling of strength ρ besides the nonreciprocal one of strength α. Further, we use two different self-interactions σ_1 and σ_2. (Although, in principle, one could still eliminate one of the σ's via a proper rescaling of time, we abstain from doing this as it is advantageous if both these parameters are able to smoothly cross zero. Specifically, all nondegenerate cases could be rescaled such that $\sigma_1 = \pm 1$.)

Furthermore, non-zero mean concentrations $\bar{u}, \bar{v}$ break the field inversion symmetry $(u, v) \rightarrow (-u, -v)$ that equivalently can be broken by introducing quadratic nonlinearities, i.e., one may employ an affine transformation $(u, v) \rightarrow (u - \bar{u}, v - \bar{v})$ to retain zero mean values but incorporate quadratic nonlinearities $3\bar{u}u^2$ and $3\bar{v}v^2$.

Linearizing about the trivial state $(u, v) = (\bar{u}, \bar{v})$ and expanding for $k \ll 1$ yields the dispersion relation (1) of the conserved-Hopf instability (see Appendix B 1). In contrast to Sec. III, here, the coefficients are

$$\mu = \frac{\sigma_1 + 3\bar{u}^2 + \sigma_2 + 3\bar{v}^2}{2}, \quad \delta' = \frac{1 + \kappa}{2},$$

$$\omega = \sqrt{\alpha^2 - \rho^2 - c^2} \quad \text{and} \quad \omega' = \frac{c(1 - \kappa)}{2\omega}, \quad (38)$$

$$\text{where} \quad c = \frac{\sigma_1 + 3\bar{u}^2 - \sigma_2 - 3\bar{v}^2}{2}.$$

Breaking the field inversion symmetry results in rather tedious calculations. Therefore, next, we focus on the case of zero mean values, i.e., Eq. (37) with $\bar{u} = \bar{v} = 0$. The consequences of lifting this restriction are discussed in the conclusion.

A. General case with field inversion symmetry

Proceeding analogously to the minimal example in Sec. III, we obtain an amplitude equation of similar form as the previous amplitude equation (17). However, due to the more general setting, the inner gradient term and the nonlinearity pick up prefactors that algebraically depend on the parameters in Eq. (38). Again, applying a Fredholm alternative at order ε^5, we obtain as amplitude equation

$$\partial_t a = \partial_{xx} \left[-\mu a - \nu \partial_{xx} a + \frac{3}{2}\gamma \left(2a\langle |a|^2 \rangle - \mathcal{F}^{-1}[\tilde{a}|\tilde{a}|^2] \right) \right], \quad (39)$$

with the complex coefficients

$$\nu = \delta' - i\omega' \quad \text{and} \quad \gamma = 1 - i\frac{c\rho}{\alpha\omega}, \quad (40)$$

where the expressions are derived in Appendix B 2. Note that the fields in Eq. (37) are scaled such that the cubic nonlinearities have prefactor one. For the amplitude equation, this implies $\text{Re}\,\gamma = 1$.

The dynamics of the amplitudes $a(x, t)$ is related to the original dynamics via the linear Schrödinger-type relation

$$\boldsymbol{u}(x, t) = e^{i\omega t\partial_{xx}} a(x, t)\boldsymbol{e}_+ + e^{-i\omega t\partial_{xx}} a^*(x, t)\boldsymbol{e}_-,$$

$$(41)$$

$$\text{with} \quad \boldsymbol{e}_\pm = \sqrt{\frac{\alpha - \rho}{2\alpha}} \begin{pmatrix} \frac{c \pm i\omega}{\alpha - \rho} \\ 1 \end{pmatrix}.$$

Here, we only discuss key properties of Eq. (39) and leave an exhaustive study of its solutions and their stability for the future. First, we note that linearizing (39) about the trivial solution $a = 0$, we obtain the dispersion relation $\lambda(k^2) = k^2\mu - \nu k^4 = k^2\mu - \delta' k^4 - i\omega' k^4$, which corresponds to Eq. (37) without the fast timescale oscillation $\sim i\omega k^2$. In other words, again, the fast timescale is fully separated and the equation only captures the slow timescale dynamics that may now include oscillations.

In the generic case, ν and γ are complex parameters and, therefore, the gradient dynamics structure shown by Eq. (16) is lost in Eq. (39). However, Eqs. (38) and (40) reveal two nongeneric cases, where the amplitude equation has a gradient dynamics structure and reduces to Eq. (16): First, if simultaneously reciprocal interactions are absent ($\rho = 0$) and the two fields have equal rigidity ($\kappa = 1$), and second if the self-interactions are symmetric ($\sigma_1 = \sigma_2$), see Table I.

Due to the complex coefficients, harmonic solutions (22) of Eq. (16) become traveling wave states $a(x, t) = a_0 \, e^{i(kx - ft)}$ for Eq. (39). Inserting this ansatz and treating real and imaginary part separately, we obtain

$$\text{Re}(39): \quad 0 = -\mu + k^2\delta' + \frac{3}{2}|a_0|^2, \quad (42)$$

$$\text{Im}(39): \quad f = k^2 \left(k^2\omega' - \frac{3}{2}|a_0|^2 \frac{c\rho}{\alpha\omega} \right). \quad (43)$$

Hence, for a traveling wave with wavenumber k, the amplitude $|a_0|$ is determined by Eq. (42) and then the frequency f is determined by Eq. (43) and features quartic and quadratic dependencies on wavenumber. Further, Eq. (42) ensures supercriticality, i.e., all bifurcations on the trivial branch are supercritical as $|a_0|^2 = 2(\mu - \mu_c)/3$ with $\mu_c = k^2\delta'$.

In terms of the fields u and v of the full nonreciprocal Cahn–Hilliard model (37), the relative modulation strength $||u||_{L^2}/||v||_{L^2}$, as well as the phase shift $\Delta\phi$ between u and v are

TABLE I. Summary of special (nongeneric) cases for the parameters of the NRCH model (37) at $\bar{u} = \bar{v} = 0$, the effect on the dispersion relation (38), and the resulting parameters in the amplitude Eq. (40). This indicates that there are two independent limiting cases where (40) reduces to (16).

| Description	Eq.(37)	Eq.(38)	Eq. (40)	Comment	
Equal rigidity	$\kappa = 1$	$\omega' = 0$	$\nu \in \mathbb{R}$		**AE**
Purely nonreciprocal coupling	$\rho = 0$		$\gamma \in \mathbb{R}$	equal modulation $||u||_{L^2} = ||v||_{L^2}$	**gradient dynamics**
Symmetric self-interaction	$\sigma_1 = \sigma_2$	$c = 0$ $\omega' = 0$	$\nu, \gamma \in \mathbb{R}$	**AE gradient dynamics** Phase shift $\Delta\phi = \pm\pi/2$	

encoded in the eigenvector e_+ in Eq. (41), namely,

$$\frac{||u||_{L^2}}{||v||_{L^2}} = \left|\frac{c \pm i\omega}{\alpha - \rho}\right| = \frac{\sqrt{\omega^2 + c^2}}{|\alpha - \rho|} = \frac{\sqrt{\alpha^2 - \rho^2}}{|\alpha - \rho|} = \sqrt{\left|\frac{\alpha + \rho}{\alpha - \rho}\right|}, \quad (44)$$

$$\tan(\Delta\phi) = \frac{\text{Im}\,\frac{c \pm i\omega}{\alpha - \rho}}{\text{Re}\,\frac{c \pm i\omega}{\alpha - \rho}} = \frac{\omega}{c}. \quad (45)$$

Hence, while purely nonreciprocal coupling ($\rho = 0$) results in identical modulation strength of u and v, any reciprocal coupling ($\rho \neq 0$) gives rise to a difference in modulation strength of the two

original fields. Equally, while identical (symmetric) self-interactions ($\sigma_1 = \sigma_2 \to c = 0$) result in a phase shift between u and v of $\pi/2$, any corresponding asymmetry ($c \neq 0$) implies a phase shift that differs from $\pi/2$. Note that the introduced measures (44) and (45) are well behaved as for a conserved-Hopf instability always $|\alpha| > |\rho|$. The nongeneric cases and the resulting consequences for the parameters on the amplitude level and the dynamics are summarized in Table I.

To test our predictions for the generic case, we fix $\mu = 1/16$ as in Fig. 5, i.e., we stay close to the onset of the conserved-Hopf instability ($\varepsilon = 1/4$), choose a generic set of parameters and a larger domain $l = 100\pi$. The results are shown in Fig. 7.
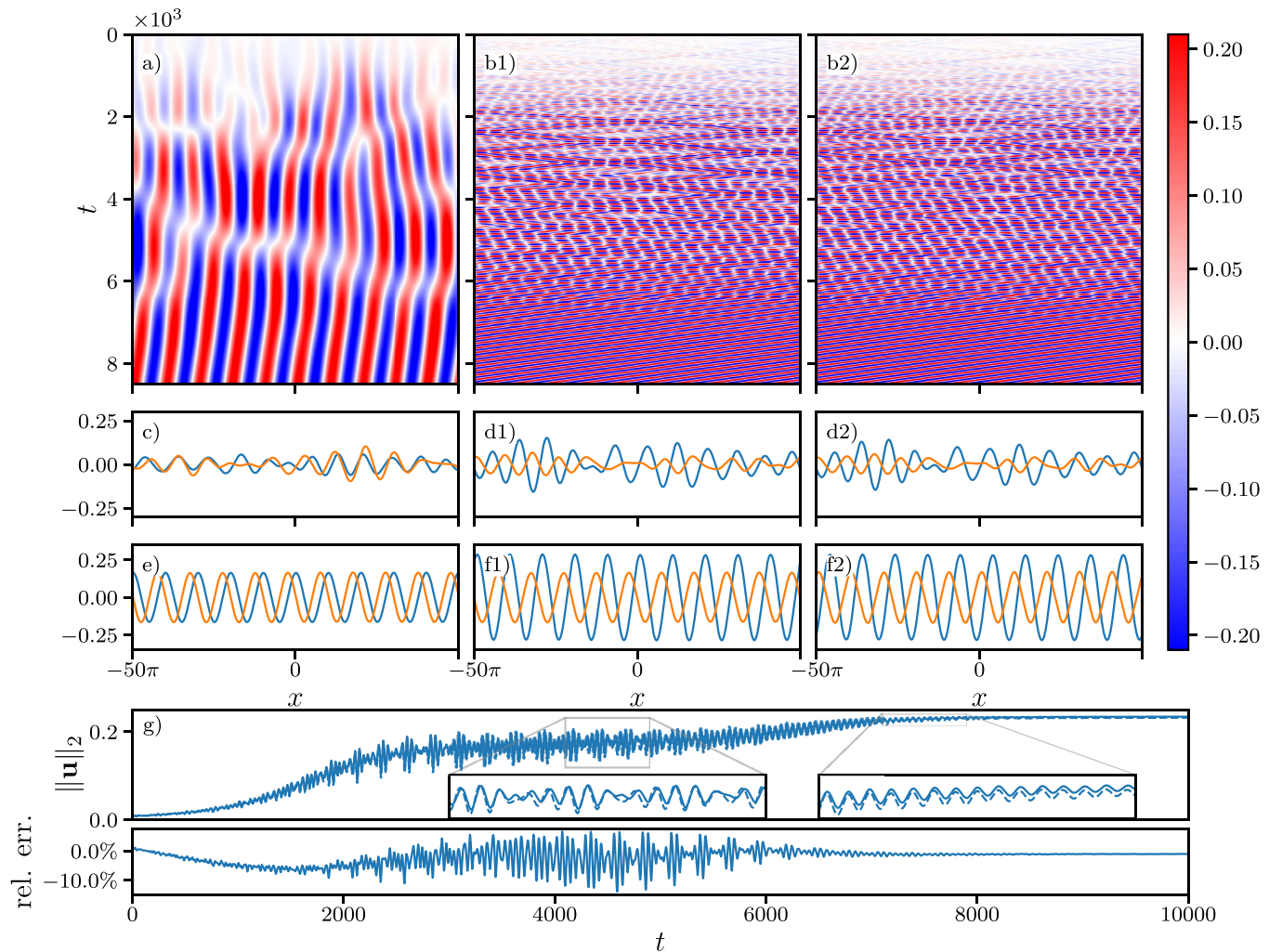
FIG. 7. Space–time plots of (a) the amplitude $\text{Im}(a)$, (b1) the dynamics of u_a reconstructed from the amplitude equation and (b2) the full dynamics u_1 of the NRCH model, all with identical white noise initial condition ($\sim 10^{-1}$). Panels (c)–(f) show corresponding example profiles at (second row) $t = 1.5 \times 10^3$ and (third row) $t = 8 \times 10^4$. The parameters are $\sigma_1 = 17/16$, $\sigma_2 = -15/16$, $\rho = 1$, $\alpha = 2$, and $\kappa = 0.1$. The corresponding parameters of the amplitude equation are $\mu = 1/16$, $\nu = 0.55 + 0.318i$, and $\gamma = 1 + 0.354i$. Panel (g) shows the temporal evolution of the L^2-norm $\|u\|_{L^2}$ of the middle (right) column as dashed (solid) lines as well as their signed relative deviation. The domain size is $l = 100\pi$ with a spatial discretisation of 2048 points and the adapted timestep is usually around 1×10^{-2} for the full dynamics and 1×10^{-1} for the amplitude equation.

Again, the reconstructed dynamics obtained via Eqs. (39) and (41) shows excellent agreement with the full model (37). Both, transients and the final states, coincide and only at very late times [$t \sim 8 \times 10^4$, panels (f1) and (f2)] the reconstructed and the full dynamics have run slightly out of phase. Further, we find the relative modulation strength of the final state, $||u||_{L^2}/||v||_{L^2} = 1.733$, to be in very good agreement with the theoretical prediction; here $\sqrt{\left|\frac{\alpha+\rho}{\alpha-\rho}\right|} = \sqrt{3} = 1.732$. Similarly, a numerical estimate of the phase shift gives $\Delta\phi = 2.160$ also in good agreement with the theoretical prediction of 2.186 obtained from Eq. (45). Numerically, we calculate the phase shift as $\cos\Delta\phi = \frac{\frac{1}{l}\int_{-l/2}^{l/2} uv\,dx}{||u||_{L^2}||v||_{L^2}}$, which becomes exact, if u and v are harmonic functions, i.e., $u = A\cos(kx + \Delta\phi)$, $v = B\cos(kx)$.

In contrast to the cases of Figs. 5 and 6, the temporal evolution of the L^2-norms is nonmonotonic and oscillatory during the transient toward a traveling wave state [Fig. 5(g)] for both the reconstructed and the full dynamics. This is closely connected to the now absent gradient dynamics structure of the amplitude equation, i.e., due to the complex coefficients. This allows for oscillatory behavior also on the slow timescale. Although the relative error is sometimes up to 15% and, therefore, larger than in the simple case treated in Secs. I–V, even the transient dynamics still qualitatively coincide [see insets in Fig. 5(g)].

VII. CONCLUSION

We have considered a large-scale oscillatory instability with conservation laws, i.e., the conserved-Hopf instability, which may occur in a wide spectrum of systems featuring (at least) two conservation laws. Examples of such systems include liquid two-layer films heated from below[51] where spatiotemporal oscillation patterns may be readily observed,[27,28] and a full cell polarity model[52] that represents a reaction–diffusion (RD) system with more than one conservation law. Recently, RD systems with conservation laws gained renewed prominence as they are highly relevant for spatiotemporal protein patterns in biochemical processes. There, reactions result in the switching of protein conformations on a timescale where the overall protein density is conserved, e.g., MinE and MinD in ATP-driven Min oscillations.[12,29,53–55] Further examples include two-species chemotactic systems,[24] mechanochemical waves in cytoskeleton and cytosol as modeled by active poroelastica,[10] oscillations in lipid-protein dynamics in cell membranes,[25] as well as liquid layers covered by self-propelled surfactants.[26]

Although such an oscillatory instability with conservation laws has been mentioned in the classification of instabilities in spatially extended systems by Cross and Hohenberg,[2] it has not yet been systematically studied. One may in general say that the role of conservation laws in pattern formation still holds quite a number of open questions.[56] A recently proposed alternative classification of instabilities in homogeneous isotropic systems into eight categories[16,34] (based on three properties: large vs small scale, stationary vs oscillatory, and nonconserved vs conserved) focused attention on the fact that weakly nonlinear theories (amplitude equations) were developed and analyzed for all of them with the exception of the conserved-Hopf instability. The general nonreciprocal Cahn–Hilliard model that was recently derived in Ref. 16 as a generic weakly nonlinear model valid in the vicinity of a conserved-Hopf instability (using n-field reaction–diffusion systems with two conservation laws as specific example to calculate all coefficients) is not an envelope equation, i.e., it does not reduce the considered time and/or length scales by describing the time evolution of the amplitudes of temporal, spatial, or spatiotemporal harmonic modes. Instead, as pointed out in the discussion of Ref. 16, it rather corresponds to an amplitude equation (of the zero-mode) on a higher level of a hierarchy of such universal equations valid in the vicinity of higher-codimension points. In consequence, it features other instabilities besides the conserved-Hopf instability, namely, conserved-Turing and Cahn–Hilliard instabilities (cf. conclusion and supplementary material of Ref. 16). Amplitude equations that are not envelope equations can arise at specific points of higher codimension where no reduction scheme based on scale separation can be employed. This occurs, e.g., at transitions between an oscillatory and a stationary instability (there, the critical frequency approaches zero, i.e., no timescale separation) or between a large-scale and a small-scale instability (critical wavenumber approaches zero, i.e., no length scale separation). The argument is further strengthened by the present work, since the complexity of the investigated NRCH models could only be reduced far away from a higher-codimension point, in particular, far away from the transition point between Cahn–Hilliard instability and conserved-Hopf instability as there the NRCH model is its own amplitude equation.[16] The general nonreciprocal Cahn–Hilliard model derived in Ref. 16 is closely related to the model proposed for oscillatory phase separation by Förtsch and Zimmermann, as documented in Ref. 42 [their GTOPS model in the forms of their Eqs. (9.3) or (9.4), also called CHEOPS[57]]. The various models with simpler local contributions to the (non)equilibrium chemical potentials and constant mobilities analyzed in Refs. 30–35 and 40 all correspond to special cases of the model derived in Ref. 16 (see their supplementary material). The simplest version that still retains the conserved-Hopf instability, features a fully linearized second equation and purely linear couplings between fields,[38,39,41,42] and is called "Minimal Model" in Ref. 42. It corresponds to the conserved equivalent of a FitzHugh–Nagumo reaction–diffusion model.

In contrast to all these studies, the present work provides a derivation and first analysis of the amplitude equation for the conserved-Hopf instability on the lowest hierarchy level, i.e., the "missing" number eight. It is an amplitude equation that corresponds to an envelope equation, i.e., it properly reduces the considered time scales by describing the evolution on the slow timescale of the amplitude of fast harmonics. Now, the obtained versions of the equation can be employed to investigate in depth the universal behavior in the vicinity of the instability onset. A key observation on the linear level has been that in the conserved case, the slow and the fast dynamics of the amplitude equation and the original system, respectively, are related via a linear Schrödinger equation, i.e., reconstructing the full multi-scale dynamics from the dynamics of the complex amplitude obtained in the weakly nonlinear model is similar to applying a quantum-mechanical time evolution operator in the case of a free-particle hamiltonian. It will be interesting to investigate in the future whether this analogy can be further exploited.

We have obtained the amplitude equation as a result of an intricate calculation up to fifth order. We have discussed it in two flavors: First, we have considered a nonreciprocal Cahn–Hilliard model with a field-exchange symmetry and purely nonreciprocal coupling and obtained the evolution equation (16) for the complex amplitude that features only real coefficients and has a gradient dynamics form. Second, breaking the field-exchange symmetry, we have obtained the evolution equation (39) for the complex amplitude that features complex coefficients and is nonvariational. In both cases, we have still assumed that the two fields of the full model have zero mean value. In Appendix B 3, we sketch the calculation for the case when this restriction is lifted. Conceptually, one again obtains an amplitude equation at order ε^5 with additional terms arising from the quadratic nonlinearity. However, as these terms are rather involved their practical use seems quite limited. The approach may now be used to analyze such equations for all mentioned versions of the nonreciprocal Cahn–Hilliard model and other more complicated models that show the conserved-Hopf instability.

Note that the operator-like relation between the levels of description was also noted by Förtsch and Zimmermann.[42,57] However, in contrast to our exact approach resulting in Eqs. (16) and (39), they Taylor-expand and truncate the exponential operator to finally obtain a local amplitude equation with ten complex parameters [Eq. (10.23) of Ref. 42] that is hard to analyze in general but still features analytic insights into certain simplified cases. It would be instructive to see a quantitative comparison of their reduced models and the dynamics of the full model.

The here-obtained amplitude equation has only a few parameters but features two types of nonlocal terms: one involves the mean value of a squared amplitude and the other is cubic in Fourier space, i.e., corresponds to a double convolution. Terms similar to the first one have also been discussed by Knobloch[18] for counterpropagating wavetrains with velocities of order one in systems without conservation laws. There, the resulting amplitude equations are two complex Ginzburg–Landau equations with mean-field coupling.[58] Such equations are also derived in the context of waves along certain combustion fronts.[59]

Analyzing the two obtained amplitude equations, we have found that the version with real coefficients has a variational structure, i.e., can be written as a gradient dynamics on the underlying energy functional (19). Further, we have shown that all its steady states can be analytically obtained as combinations of harmonic modes with amplitudes given as solutions of an inhomogeneous linear system of equations. They correspond to various wave states of the full dynamics. The energy functional allows one to predict which wave state will ultimately be selected in a long-time limit. For wave number q, the single-mode states correspond to a mean energy density of $\mathcal{G}/l = -(\mu - q^2)^2/3$, i.e., the domain-filling mode always ultimately dominates. The full spectrum of all energies of steady states included in Fig. 4(a) is given in Fig. 8 using identical line styles. We believe that the two-mode state that bifurcates from a one-mode state at the respective final stabilizing pitchfork bifurcation corresponds to the threshold state that has to be overcome to transition to a state of lower energy. Therefore, the corresponding nondimensional energy difference $\Delta\mathcal{G}$ will allow one to obtain an estimate for the probability of remaining in a local energy minimum
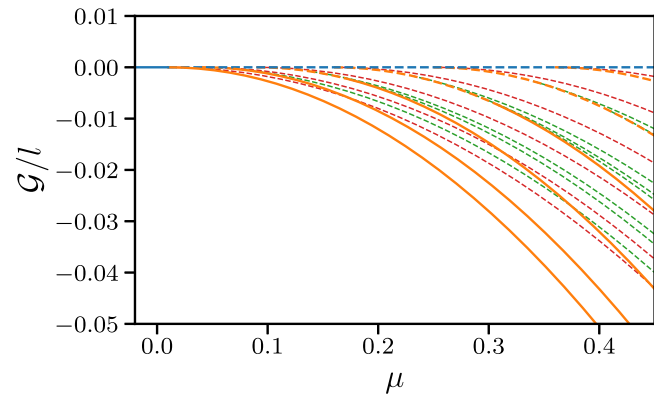

FIG. 8. Energy density $\mathcal{G}/l$, i.e., Eq. (19), for all steady states of the amplitude equation (16) that are included in Fig. 4(a) shown here with identical line styles.

[as $1 - \exp(-\Delta\mathcal{G})$]. Additionally, we have determined the linear stability of single-mode states. The obtained dispersion relation for perturbations of the single-mode state shows that it is a stationary large-scale instability not unlike the Eckhaus instability,[3] however, with a different prefactor in the condition for onset and a different meaning of the wavenumber of the considered mode. For the Eckhaus instability, it corresponds to the offset with respect to the finite critical wavenumber while here it is the offset with respect to zero. A subsequent comparison of analytically and numerically obtained bifurcation diagrams for the steady states of the amplitude equation and the traveling waves of the full model, respectively, has shown excellent agreement with only small differences emerging when moving away from the onset of the first mode. We have also compared transient dynamics for various initial conditions and also found very good agreement. Further, in our time simulations on the level of the amplitude equation, we have observed the expected reduction in numerical effort as compared to the full model. The expected ratio of characteristic timesteps on the two levels of description roughly corrresponds to the factor ε^2 between fast and slow timescales.

The generic amplitude equation with complex coefficients has a nonvariational structure. Here, we have only analytically determined single-mode traveling wave states of the amplitude equation. Further, we have compared the transient toward such a state as obtained from the reconstructed dynamics of the amplitude equation and from the full model. Also, here the agreement has been very good. A discussion of further states and of their stability is left for the future. It will be particularly interesting to explore whether the derived complex equation allows for chaotic dynamics similar to its counterpart for nonconserved dynamics, the complex Ginzburg–Landau equation.[17]

In general, we believe that the approach can be further developed in several directions: On the one hand, employing a more general scaling (i.e., not fixing the prefactors of the cubic terms to one), one can assess how the amplitude equation simplifies when considering the above discussed simplest version of the NRCH model that still retains the conserved-Hopf instability, recently analyzed in

some detail in Ref. 41. One the other hand, further cubic coupling terms may be introduced into the derivation, e.g., to assess how the parameters of the complex amplitude equation change when considering the complex Cahn–Hilliard equation that is a limiting case of a model studied in Ref. 60 or other versions of the NRCH model considered in Refs. 30–32, 40, and 61.

Finally, we point out that Ref. 27 presents a review of mainly hydrodynamic models with conservation laws that show large-scale oscillatory behavior "outside the world of the complex Ginzburg–Landau equation." Specifically, similar oscillatory instabilities as the one discussed here occur in a liquid confined between two plates in Refs. 27 and 62, where the conservation of a concentration field and the approximate conservation of temperature in the limit of small Biot numbers can give rise to a large scale oscillatory instability. References 27 and 62 discuss several weakly and strongly nonlinear approaches, and it will be interesting to determine detailed relations to the here discussed real and complex versions of the amplitude equation for the conserved-Hopf instability. In particular, Ref. 62 presents an amplitude equation that has a limiting case similar to the equation obtained and analyzed here.

Overall, the approach we have presented may prove useful to gain a more unified understanding of all mentioned cases of large-scale oscillatory pattern formation.

AUTHOR DECLARATIONS

Conflict of Interest

The authors have no conflicts to disclose.

Author Contributions

Daniel Greve: Conceptualization (equal); Data curation (lead); Formal analysis (equal); Investigation (lead); Software (lead); Visualization (lead); Writing – original draft (equal); Writing – review & editing (equal). **Uwe Thiele:** Conceptualization (equal); Formal analysis (equal); Funding acquisition (lead); Project administration (equal); Supervision (lead); Writing – original draft (equal); Writing – review & editing (equal).

DATA AVAILABILITY

The data that support the findings of this study are openly available on zenodo at https://doi.org/10.5281/zenodo.14218246, in Ref. 63.

APPENDIX A: CLASSIFICATION INTO EIGHT INSTABILITY TYPES

Table II lists the eight instability types alluded to in Sec. I and their relation to the traditional classification. Each of eight types is characterized by the linear modes that dominate at and close to the corresponding instability threshold. Here, we also follow the naming convention given in the table. The traditional classification by Cross and Hohenberg[2] only distinguishes six cases. It is included for reference. We remark that the statement "type II can often be scaled to resemble type I" on page 870 of Ref. 2 is not correct, otherwise Cahn–Hilliard and Swift–Hohenberg equations would have similar dynamics close to onset. Furthermore, their remarks on frequencies in the context of the oscillatory case II should be replaced by the present discussion in Sec. II.

APPENDIX B: CALCULATIONS FOR THE GENERIC CASE

In Sec. III, we have explained how to derive the amplitude equation (16) as weakly nonlinear model in the vicinity of a conserved-Hopf bifurcation for a nonreciprocal Cahn–Hilliard

TABLE II. Overview of the classification and employed naming convention of linear instabilities and corresponding bifurcations of spatially extended homogeneous isotropic systems based on the three dichtomous properties: large-scale (L) vs small-scale (S) instability, stationary (s) vs oscillatory (o) instability, and nonconserved (N) vs conserved (C) dynamics of relevant linear mode(s). For comparison, in parentheses, the (incomplete) classification of Cross and Hohenberg[2] is also given. Reprinted with permission from Frohoff-Hülsmann and Thiele, Phys. Rev. Lett. **131**, 107201 (2023).[16] Copyright 2024 the American Physical Society. Also, see the discussion in Ref. 34.

	Nonconserved dynamics	Conserved dynamics
Homogeneous/large-scale, stationary	Allen–Cahn (III$_s$)	Cahn–Hilliard (II$_s$)
Homogeneous/large-scale, oscillatory	Hopf[a] (III$_o$)	Conserved-Hopf (II$_o$)
Small-scale, stationary	Turing (I$_s$)	Conserved-Turing (–)
Small-scale, oscillatory	Wave[b] (I$_o$)	Conserved-wave (–)

[a] Also known as "Poincaré–Andronov–Hopf."
[b] Also called "finite-wavelength Hopf" or "oscillatory Turing."

05 December 2024 16:45:27

model with a field inversion symmetry and an additional field-exchange symmetry. Here, we generalize the procedure to the case where the field-exchange symmetry is broken, i.e., we show how to obtain the version with complex coefficients (39) as amplitude equation in the vicinity of the conserved-Hopf bifurcation for the more general nonreciprocal Cahn–Hilliard model (37).

1. Dispersion relation

Inserting the ansatz $\boldsymbol{u} = \boldsymbol{u}_0 + \varepsilon\, e^{ikx+\lambda t}\delta\boldsymbol{u}$, with $\boldsymbol{u}_0 = (\bar{u}, \bar{v})$ into (37) and linearizing in ε yields the linear eigenvalue problem

$$\lambda\delta\boldsymbol{u} = k^2 \begin{pmatrix} \sigma_1 + 3\bar{u}^2 - k^2 & (\rho + \alpha) \\ (\rho - \alpha) & \sigma_2 + 3\bar{v}^2 - \kappa k^2 \end{pmatrix}\delta\boldsymbol{u}, \qquad (B1)$$

with eigenvalues

$$\lambda_{1,2}(k^2) = k^2 \left[\mu - \delta' k^2 \pm \sqrt{(c - \tilde{c}k^2)^2 + \rho^2 - \alpha^2} \right], \qquad (B2)$$

where we introduced

$$\mu = \frac{\sigma_1 + 3\bar{u}^2 + \sigma_2 + 3\bar{v}^2}{2}, \quad \delta' = \frac{1+\kappa}{2},$$
$$c = \frac{\sigma_1 + 3\bar{u}^2 - \sigma_2 - 3\bar{v}^2}{2}, \quad \tilde{c} = \frac{1-\kappa}{2}. \qquad (B3)$$

The condition for large-scale oscillatory modes is a negative discriminant at $k^2 \ll 1$, i.e., the contribution of the nonreciprocal coupling α^2 has to be sufficiently large. Expanding the root in (B2) for $k^2 \ll 1$, we obtain

$$\lambda_{1,2}(k^2) = k^2 \left[\mu - \delta' k^2 \pm i\left(\omega - \omega' k^2\right) \right], \qquad (B4)$$

where we have furthermore introduced

$$\omega = \sqrt{\alpha^2 - \rho^2 - c^2}, \quad \omega' = \frac{c\tilde{c}}{\omega}. \qquad (B5)$$

This corresponds to the dispersion relation (1) without the $\mathcal{O}(k^6)$ terms that are not relevant for our calculation. The system is close to the onset of a conserved-Hopf instability if $|\mu| \ll 1$ and $\omega = \mathcal{O}(1)$.

2. Case of intact field inversion symmetry

First, we retain the field inversion symmetry by assuming $\bar{v} = \bar{u} = 0$. Using the introduced parametrization, the system reads

$$\partial_t \boldsymbol{u} = \underline{\boldsymbol{D}}\partial_{xx}\boldsymbol{u} - \underline{\boldsymbol{D}}_2 \partial_{xxxx}\boldsymbol{u} + \partial_{xx}\boldsymbol{N}_3(\boldsymbol{u}) - \mu\partial_{xx}\boldsymbol{u},$$

$$\text{with} \quad \underline{\boldsymbol{D}} = \begin{pmatrix} c & -(\rho+\alpha) \\ -(\rho-\alpha) & -c \end{pmatrix}, \quad \underline{\boldsymbol{D}}_2 = \begin{pmatrix} 1 & 0 \\ 0 & \kappa \end{pmatrix}, \quad (B6)$$

$$\text{and} \quad \boldsymbol{N}_3(\boldsymbol{u}) = \begin{pmatrix} u^3 \\ v^3 \end{pmatrix}.$$

Then, we again formally expand the field in orders of $\varepsilon = \sqrt{|\mu|}$ and introduce the scalings $\partial_t = \varepsilon^2\partial_\tau + \varepsilon^4\partial_T$ and $\partial_x = \varepsilon\partial_X$ with $\boldsymbol{u} = \varepsilon\boldsymbol{u}_1(X, \tau, T) + \text{h.o.t.}$ We start solving Eq. (B6) order by order. The linear equation arising at $\mathcal{O}(\varepsilon^3)$ reads

$$\underline{\boldsymbol{L}}\boldsymbol{u}_1 = 0, \quad \text{with} \quad \underline{\boldsymbol{L}} = \underline{\boldsymbol{1}}\partial_\tau - \underline{\boldsymbol{D}}\partial_{XX}. \qquad (B7)$$

This equation is of linear Schrödinger-type and solved by

$$\boldsymbol{u}_1 = e^{i\omega\tau\partial_{XX}}A(X, T)\boldsymbol{e}_+ + \text{c.c.},$$
$$\boldsymbol{e}_\pm = \sqrt{\frac{\alpha-\rho}{2\alpha}}\begin{pmatrix} \frac{c \pm i\omega}{\alpha-\rho} \\ 1 \end{pmatrix}, \qquad (B8)$$

where $\boldsymbol{e}_\pm$ are normalized eigenvectors of $\underline{\boldsymbol{D}}$ with eigenvalues $\pm i\omega$. To apply the Fredholm alternative at higher orders, we need the kernel of the adjoint linear operator $\underline{\boldsymbol{L}}^\dagger = -\underline{\boldsymbol{1}}\partial_\tau - \underline{\boldsymbol{D}}^\dagger\partial_{XX}$. The modes in the kernel are given by

$$\boldsymbol{m} = e^{i\omega\tau\partial_{XX}}B(X)\boldsymbol{e}_+^\dagger + e^{-i\omega\tau\partial_{XX}}C(X)\boldsymbol{e}_-^\dagger,$$
$$\text{with} \quad \boldsymbol{e}_\pm^\dagger = \sqrt{\frac{\alpha+\rho}{2\alpha}}\begin{pmatrix} \frac{-c \pm i\omega}{\alpha+\rho} \\ 1 \end{pmatrix}, \qquad (B9)$$

where $\boldsymbol{e}_\pm^\dagger$ are eigenvectors of $\underline{\boldsymbol{D}}^\dagger$ with eigenvalues $\mp i\omega$. Further note that $\langle\boldsymbol{e}_+^\dagger; \boldsymbol{e}_-\rangle = 0$. Hence, we can project Eq. (B8) onto the amplitude $A(\hat{X}, T)$ using $B(X) = \delta(X - \hat{X})$ and $C(X) = 0$.

At $\mathcal{O}(\varepsilon^5)$, we obtain the system

$$\underline{\boldsymbol{L}}\boldsymbol{u}_3 = -\underline{\boldsymbol{D}}_2\partial_{XXXX}\boldsymbol{u}_1 - \tilde{\mu}\partial_{XX}\boldsymbol{u}_1 - \partial_T\boldsymbol{u}_1 + \partial_{XX}\boldsymbol{N}_3(\boldsymbol{u}_1). \qquad (B10)$$

As in the main text, we treat linear and nonlinear terms separately. For the linear terms, the Fredholm alternative yields

$$0 = \langle e^{i\omega\tau\partial_{XX}}\delta(X - \hat{X})\boldsymbol{e}_+^\dagger; (-\underline{\boldsymbol{D}}_2\partial_{XXXX}\boldsymbol{u}^{(1)} - \tilde{\mu}\partial_{XX}\boldsymbol{u}^{(1)} - \partial_T\boldsymbol{u}_1)\boldsymbol{e}_+\rangle$$

$$\Leftrightarrow \quad \langle\boldsymbol{e}_+^\dagger; \boldsymbol{e}_+\rangle\partial_T A = -\langle\boldsymbol{e}_+^\dagger; \underline{\boldsymbol{D}}_2\boldsymbol{e}_+\rangle\partial_{\hat{X}\hat{X}\hat{X}\hat{X}}A - \langle\boldsymbol{e}_+^\dagger; \boldsymbol{e}_+\rangle\tilde{\mu}\partial_{\hat{X}\hat{X}}A. \qquad (B11)$$

Next, we deal with the cubic contributions $\partial_{XX}\boldsymbol{N}_3(\boldsymbol{u})$. Expressed by the amplitudes, they read

$$\partial_{XX}\boldsymbol{N}_3(\boldsymbol{u}) = \partial_{XX}\begin{pmatrix} u_1^3 \\ v_1^3 \end{pmatrix} = \partial_{XX}\left[\left(e^{i\omega\tau\partial_{XX}}A(X, T)\right)^3 \boldsymbol{w}^{(1)} \right.$$

$$+ 3\left(e^{-i\omega\tau\partial_{XX}}A^*(X, T)\right)\left(e^{i\omega\tau\partial_{XX}}A(X, T)\right)^2 \boldsymbol{w}^{(2)}$$

$$+ 3\left(e^{-i\omega\tau\partial_{XX}}A^*(X, T)\right)^2\left(e^{i\omega\tau\partial_{XX}}A(X, T)\right) \boldsymbol{w}^{(3)}$$

$$\left. + \left(e^{-i\omega\tau\partial_{XX}}A^*(X, T)\right)^3 \boldsymbol{w}^{(4)} \right], \qquad (B12)$$

where $\boldsymbol{w}^{(i)}$ are given by

$$\boldsymbol{w}^{(1)} = \begin{pmatrix} (\boldsymbol{e}_+)_1^3 \\ (\boldsymbol{e}_+)_2^3 \end{pmatrix}, \quad \boldsymbol{w}^{(2)} = \begin{pmatrix} (\boldsymbol{e}_+)_1^2(\boldsymbol{e}_-)_1 \\ (\boldsymbol{e}_+)_2^2(\boldsymbol{e}_-)_2 \end{pmatrix},$$

$$\boldsymbol{w}^{(3)} = \begin{pmatrix} (\boldsymbol{e}_+)_1(\boldsymbol{e}_-)_1^2 \\ (\boldsymbol{e}_+)_2(\boldsymbol{e}_-)_2^2 \end{pmatrix}, \quad \text{and} \quad \boldsymbol{w}^{(4)} = \begin{pmatrix} (\boldsymbol{e}_-)_1^3 \\ (\boldsymbol{e}_-)_2^3 \end{pmatrix}. \qquad (B13)$$

The Fredholm alternative for the term $\sim \boldsymbol{w}^{(2)}$ then yields the contribution

$$3\left\langle e^{\mathrm{i}\omega\tau\partial_{XX}}\delta(X-\hat{X})\boldsymbol{e}_+^\dagger; \partial_{XX}\left(e^{-\mathrm{i}\omega\tau\partial_{XX}}A^*(X,T)\right)\left(e^{\mathrm{i}\omega\tau\partial_{XX}}A(X,T)\right)^2\boldsymbol{w}^{(2)}\right\rangle$$

$$= \frac{3}{2}\left\langle e^{\mathrm{i}\omega\tau\partial_{XX}}\sum_Q e^{\mathrm{i}Q(X-\hat{X})}\boldsymbol{e}_+^\dagger; \partial_{XX}\left(e^{-\mathrm{i}\omega\tau\partial_{XX}}\sum_K \tilde{A}^*(K,T)\,e^{-\mathrm{i}KX}\right)\left(e^{\mathrm{i}\omega\tau\partial_{XX}}\sum_K \tilde{A}(K,T)\,e^{\mathrm{i}KX}\right)^2\boldsymbol{w}^{(2)}\right\rangle$$

$$= \frac{3\Omega_{\min}}{L}\langle\boldsymbol{e}_+^\dagger; \boldsymbol{w}^{(2)}\rangle\sum_{Q,K,K',K''}e^{\mathrm{i}Q\hat{X}}\tilde{A}^*(K,T)\tilde{A}(K',T)\tilde{A}(K'',T)\,(-Q^2)\int_0^{1/\Omega_{\min}}e^{\mathrm{i}\omega\tau(Q^2+K^2-K'^2-K''^2)}\,\mathrm{d}\tau\int_0^L e^{\mathrm{i}X(-Q-K+K'+K'')}\,\mathrm{d}X$$

$$= 3\langle\boldsymbol{e}_+^\dagger; \boldsymbol{w}^{(2)}\rangle\left[2\sum_Q e^{\mathrm{i}Q\hat{X}}(-Q^2)\tilde{A}(Q,T)\sum_K \tilde{A}^*(K,T)\tilde{A}(K,T) - \sum e^{\mathrm{i}QX'}(-Q^2)\tilde{A}(Q,T)\tilde{A}(Q,T)\tilde{A}^*(Q,T)\right]$$

$$= 3\langle\boldsymbol{e}_+^\dagger; \boldsymbol{w}^{(2)}\rangle\partial_{\hat{X}\hat{X}}\left(2\mathcal{F}^{-1}[\tilde{A}(K,T)\sum_{K'}|\tilde{A}(K',T)|^2] - \mathcal{F}^{-1}[\tilde{A}(K,T)|\tilde{A}(K,T)|^2]\right). \tag{B14}$$

Collecting all terms and introducing the original scales, we obtain the amplitude equation

$$\partial_t a = \partial_{xx}\left[-\mu a - \nu\partial_{xx}a + \frac{3}{2}\gamma\left(2a\langle|a|^2\rangle - \mathcal{F}^{-1}[\tilde{a}|\tilde{a}|^2]\right)\right], \tag{B15}$$

where the general complex coefficients are given as

$$\nu = \frac{1}{\langle\boldsymbol{e}_+^\dagger; \boldsymbol{e}_+\rangle}\langle\boldsymbol{e}_+^\dagger; \underline{\mathbf{D}}_2\boldsymbol{e}_+\rangle = \delta' - \mathrm{i}\omega',$$

$$\gamma = \frac{2}{\langle\boldsymbol{e}_+^\dagger; \boldsymbol{e}_+\rangle}\langle\boldsymbol{e}_+^\dagger; \boldsymbol{w}^{(2)}\rangle = 1 - \mathrm{i}\frac{c\rho}{\alpha\omega}. \tag{B16}$$

The particular coefficients arise from the NRCH model (37), i.e.,

$$\langle\boldsymbol{e}_+^\dagger; \boldsymbol{e}_+\rangle = \sqrt{\frac{\alpha+\rho}{2\alpha}}\sqrt{\frac{\alpha-\rho}{2\alpha}}\left(\frac{-c-\mathrm{i}\omega}{\alpha+\rho}\frac{c+\mathrm{i}\omega}{\alpha-\rho}+1\right)$$

$$= \frac{\sqrt{\alpha^2-\rho^2}}{2\alpha}\frac{\omega^2-c^2+\alpha^2-\rho^2-2\mathrm{i}\omega c}{\alpha^2-\rho^2} = \frac{\omega^2-\mathrm{i}\omega c}{\alpha\sqrt{\alpha^2-\rho^2}},$$

$$\langle\boldsymbol{e}_+^\dagger; \underline{\mathbf{D}}_2\boldsymbol{e}_+\rangle = \sqrt{\frac{\alpha+\rho}{2\alpha}}\sqrt{\frac{\alpha-\rho}{2\alpha}}\left(\frac{-c-\mathrm{i}\omega}{\alpha+\rho}\frac{c+\mathrm{i}\omega}{\alpha-\rho}+\kappa\right)$$

$$= \frac{\sqrt{\alpha^2-\rho^2}}{2\alpha}\frac{\omega^2-c^2+\kappa(\alpha^2-\rho^2)-2\mathrm{i}\omega c}{\alpha^2-\rho^2}$$

$$= \frac{\omega^2\frac{(1+\kappa)}{2}-c^2\frac{(1-\kappa)}{2}-\mathrm{i}\omega c}{\alpha\sqrt{\alpha^2-\rho^2}}$$

$$\implies \nu = \frac{\omega^2\frac{(1+\kappa)}{2}-c^2\frac{(1-\kappa)}{2}-\mathrm{i}\omega c}{\omega^2-\mathrm{i}\omega c}$$

$$= \frac{1}{\omega^4+\omega^2 c^2}\left[\omega^4\frac{(1+\kappa)}{2}+\omega^2 c^2\frac{(1-\kappa)}{2}+\omega^2 c^2+\mathrm{i}\omega c\left(\omega^2\frac{(1+\kappa)}{2}-c^2\frac{(1-\kappa)}{2}-\omega^2\right)\right]$$

$$= \delta' - \mathrm{i}\omega', \tag{B17}$$

$$\langle \boldsymbol{e}_+^\dagger ; \boldsymbol{w}^{(2)} \rangle = \sqrt{\frac{\alpha+\rho}{2\alpha}} \sqrt{\frac{\alpha-\rho}{2\alpha}}^3 \left[\frac{-c-\mathrm{i}\omega}{\alpha+\rho} \left(\frac{c+\mathrm{i}\omega}{\alpha-\rho} \right)^2 \frac{c-\mathrm{i}\omega}{\alpha-\rho} + 1 \right]$$

$$= \frac{\sqrt{\alpha^2-\rho^2}(\alpha-\rho)}{4\alpha^2} \left[\frac{(\omega^2+c^2)(\omega^2-c^2-2\mathrm{i}\omega c)}{(\alpha^2-\rho^2)(\alpha-\rho)^2} + 1 \right]$$

$$= \frac{\sqrt{\alpha^2-\rho^2}}{4\alpha^2(\alpha-\rho)} \left[\omega^2 - c^2 - 2\mathrm{i}\omega c + (\alpha-\rho)^2 \right]$$

$$= \frac{\sqrt{\alpha^2-\rho^2}}{2\alpha^2(\alpha-\rho)} \left[\alpha^2 - c^2 - \rho\alpha - \mathrm{i}\omega c \right]$$

$$\implies \quad \gamma = \frac{2(\alpha^2-\rho^2)}{2\alpha(\alpha-\rho)} \frac{\alpha^2 - c^2 - \rho\alpha - \mathrm{i}\omega c}{\omega^2 - \mathrm{i}\omega c}$$

$$= \frac{\alpha+\rho}{\alpha\omega} \frac{1}{\omega^2+c^2} \left[\omega\alpha^2 - \omega c^2 - \rho\alpha\omega + \omega c^2 + \mathrm{i}\omega c(\alpha^2 - c^2 - \rho\alpha - \omega^2) \right]$$

$$= 1 - \mathrm{i}\frac{c\rho}{\alpha\omega}.$$

3. Case of broken field inversion symmetry

Finally, we break the field inversion symmetry by assuming $\bar{v} \neq 0$ and $\bar{u} \neq 0$. We use an affine transformation $(\hat{u}(x,t), \hat{v}(x,t)) = (u(x,t) - \bar{u}, v(x,t) - \bar{v})$, where the new fields (with hat) represent the deviations from the average of the old fields. From Eq. (37), we obtain the system

$$\partial_t \hat{u} = \partial_{xx} \left[(\sigma_1 + 3\bar{u}^2)\hat{u} + 3\bar{u}\hat{u}^2 + \hat{u}^3 - \partial_{xx}\hat{u} - (\rho+\alpha)\hat{v} \right],$$

$$\partial_t \hat{v} = \partial_{xx} \left[(\sigma_2 + 3\bar{v}^3)\hat{v} + 3\bar{v}\hat{v}^2 + \hat{v}^3 - \kappa\partial_{xx}\hat{v} - (\rho-\alpha)\hat{u} \right], \tag{B18}$$

$$\text{with} \quad \frac{1}{l}\int_0^l \hat{u}\,\mathrm{d}x = 0 \quad \text{and} \quad \frac{1}{l}\int_0^l \hat{v}\,\mathrm{d}x = 0,$$

where we already dropped all constant terms from the brackets as they are eliminated by the outer derivatives. Dropping the hats, the system reads

$$\partial_t \boldsymbol{u} = \underline{\mathbf{D}}\partial_{xx}\boldsymbol{u} - \underline{\mathbf{D}}_2 \partial_{xxxx}\boldsymbol{u} + \partial_{xx}\boldsymbol{N}_2(\boldsymbol{u}) + \partial_{xx}\boldsymbol{N}_3(\boldsymbol{u}) - \mu\partial_{xx}\boldsymbol{u},$$

$$\text{with} \quad N_2(\boldsymbol{u}) = \begin{pmatrix} 3\bar{u}u^2 \\ 3\bar{v}v^2 \end{pmatrix}. \tag{B19}$$

The remaining expressions $(\underline{\mathbf{D}}, \underline{\mathbf{D}}_2, N_2(\boldsymbol{u}))$ are as in Eq. (B6), i.e., the quadratic nonlinearity $\partial_{xx}N_2(\boldsymbol{u})$ is the only difference to the previous case. The linear problem at $\mathcal{O}(\varepsilon)$ is the same as before. However, now we have to refine our ansatz to $\boldsymbol{u} = \varepsilon\boldsymbol{u}_1 + \varepsilon^2\boldsymbol{u}_2$ to deal with the inhomogeneity that appears at $\mathcal{O}(\varepsilon^4)$, where the corresponding equation reads

$$\underline{\mathbf{L}}\boldsymbol{u}_2 = \partial_{XX}\boldsymbol{N}_2(\boldsymbol{u}_1). \tag{B20}$$

The Fredholm alternative at $\mathcal{O}(\varepsilon^4)$ is automatically fulfilled. To demonstrate this, we pick an arbitrary quadratic term in the amplitudes that arises after inserting the amplitudes $\boldsymbol{u}_1$ into $\boldsymbol{N}_2(\boldsymbol{u}_1(X, \tau, \tau'))$ and multiplying out the binomial,

$$\left\langle \boldsymbol{m}; \partial_{XX}\left(e^{-\mathrm{i}\hat{\omega}\tau}A^*(X,T) \right)\left(e^{\mathrm{i}\hat{\omega}\tau}A(X,T) \right)\tilde{\boldsymbol{w}} \right\rangle$$

$$= \left\langle e^{\mathrm{i}\omega\tau\partial_{XX}}\sum_Q e^{\mathrm{i}Q(X-X')}\boldsymbol{e}_+^\dagger ; \partial_{XX}\left(e^{-\mathrm{i}\omega\tau\partial_{XX}}\sum_K \tilde{A}^*(K,T)\,e^{-\mathrm{i}KX} \right)\left(e^{\mathrm{i}\omega\tau\partial_{XX}}\sum_K \tilde{A}(K,T)\,e^{\mathrm{i}KX} \right)\tilde{\boldsymbol{w}} \right\rangle$$

$$\sim \sum_{Q,K,K'} e^{\mathrm{i}QX'}\tilde{A}^*(K,T)\tilde{A}(K',T)\left(-(Q)^2 \right) \int e^{\mathrm{i}\omega\tau(Q^2+K^2-K'^2)}\,\mathrm{d}\tau \int e^{\mathrm{i}X(Q+K-K')}\,\mathrm{d}X. \tag{B21}$$

Hence, nonzero contributions have to fulfill

$$Q^2 + K^2 - K'^2 = 0 \quad \text{and} \quad Q + K - K' = 0, \tag{B22}$$

which can only hold if either $Q = 0$ and $K = K'$ or $K = 0$ and $Q = K'$. The two terms do not contribute as the first one vanishes due to the factor Q^2 in (B21) and the second one as $\tilde{A}^*(0, T) = 0$. A similar argument holds for all contributions in N_2. Hence, the solvability conditon is always fulfilled. In other words, there is no nontrivial elastic $1 \to 2$ or $2 \to 1$ scattering process of particles with equal mass in one dimension.

To solve the inhomogeneous linear partial differential equation (PDE) (B20) at $\mathcal{O}(\varepsilon^4)$, we insert the Fourier-transformed amplitudes into N_2 and express the vectorial parts in the basis $\{e_+, e_-\}$,

$$
\begin{aligned}
N_2 = \begin{pmatrix} 3\bar{u}u_1^2 \\ 3\bar{v}v_1^2 \end{pmatrix} &= \sum_{K'K''} A(K')A(K'') \, e^{iX(K'+K'')} \, e^{-i\omega\tau(K'^2+K''^2)} \begin{pmatrix} 3\bar{u}(e_+)_1^2 \\ 3\bar{v}(e_+)_2^2 \end{pmatrix} \\
&\quad + 2\sum_{K'K''} \tilde{A}(K')\tilde{A}^*(K'') \, e^{iX(K'-K'')} \, e^{-i\omega\tau(K'^2-K''^2)} \begin{pmatrix} 3\bar{u}(e_+)_1(e_-)_1 \\ 3\bar{v}(e_+)_2(e_-)_2 \end{pmatrix} \\
&\quad + \sum_{K'K''} \tilde{A}^*(K')\tilde{A}^*(K'') \, e^{iX(-K'-K'')} \, e^{i\omega\tau(K'^2+K''^2)} \begin{pmatrix} 3\bar{u}(e_-)_1^2 \\ 3\bar{v}(e_-)_2^2 \end{pmatrix} \\
&= \sum_{K'K''} \tilde{A}(K')\tilde{A}(K'') \, e^{iX(K'+K'')} \, e^{-i\omega\tau(K'^2+K''^2)} (\eta_1 e_+ + \eta_2 e_-) \\
&\quad + 2\sum_{K'K''} \tilde{A}(K')\tilde{A}^*(K'') \, e^{iX(K'-K'')} \, e^{-i\omega\tau(K'^2-K''^2)} (\eta_3 e_+ + \eta_3^* e_-) \\
&\quad + \sum_{K'K''} \tilde{A}^*(K')\tilde{A}^*(K'') \, e^{iX(-K'-K'')} \, e^{i\omega\tau(K'^2+K''^2)} (\eta_2^* e_+ + \eta_1^* e_-),
\end{aligned}
\tag{B23}
$$

where the coefficients are given by

$$\eta_1 = \frac{3\alpha}{i\omega} (\bar{u}(e_+)_1^2(e_-)_2 - \bar{v}(e_+)_2^2(e_-)_1),$$

$$\eta_2 = -\frac{3\alpha}{i\omega} (\bar{u}(e_+)_1^2(e_+)_2 - \bar{v}(e_+)_2^2(e_+)_1), \tag{B24}$$

$$\eta_3 = \frac{3\alpha}{i\omega} (\bar{v}(e_+)_2(e_-)_2(e_-)_1 - \bar{u}(e_+)_1(e_-)_1(e_-)_2).$$

The occurence of the complex conjugated factors arises from the fact that $N_2 \in \mathbb{R}^2$.

We can then find a solution for each contribution, e.g., for the first term, we employ the ansatz

$$u_2 \sim \sum_{K'K''} f(K', K'') \, e^{iX(K'+K'')} \, e^{-i\omega\tau(K'^2+K''^2)} e_+. \tag{B25}$$

Then, applying $\underline{L}$, we obtain

$$\underline{L}u_2 = \sum_{K'K''} f(K', K'') i\omega \left[(K' + K'')^2 - (K'^2 + K''^2) \right] e^{iX(K'+K'')} \, e^{-i\omega\tau(K'^2+K''^2)} e_+, \tag{B26}$$

and comparison to the first term in $\partial_{XX}N_2$ yields that

$$f(K', K'') = \frac{\eta_1}{i\omega} \tilde{A}(K')\tilde{A}(K'') \frac{-(K' + K'')^2}{(K' + K'')^2 - (K'^2 + K''^2)}. \tag{B27}$$

Therefore, we find the solution

$$
\begin{aligned}
\boldsymbol{u}_2 &= \sum_{K',K''} \frac{1}{i\omega} \left\{ \tilde{A}(K')\tilde{A}(K'')\, e^{iX(K'+K'')}\, e^{-i\omega\tau(K'^2+K''^2)}(K'+K'')^2 \left[\frac{\eta_1}{(K'^2+K''^2)-(K'+K'')^2}\boldsymbol{e}_+ + \frac{\eta_2}{(K'^2+K''^2)+(K'+K'')^2}\boldsymbol{e}_- \right] \right. \\
&\quad + 2\tilde{A}(K')\tilde{A}^*(K'')\, e^{iX(K'-K'')}\, e^{-i\omega\tau(K'^2-K''^2)}(K'-K'')^2 \left[\frac{\eta_3}{(K'^2-K''^2)-(K'-K'')^2}\boldsymbol{e}_+ + \frac{\eta_3^*}{(K'^2-K''^2)+(K'-K'')^2}\boldsymbol{e}_- \right] \\
&\quad \left. + \tilde{A}^*(K')\tilde{A}^*(K'')\, e^{iX(-K'-K'')}\, e^{-i\omega\tau(-K'^2-K''^2)}(K'+K'')^2 \left[\frac{\eta_2^*}{(K'^2+K''^2)+(K'+K'')^2}\boldsymbol{e}_+ + \frac{\eta_1^*}{-(K'^2+K''^2)+(K+K'')^2}\boldsymbol{e}_- \right] \right\} \\
&= \sum_{K',K''} \frac{1}{2i\omega} \left\{ \tilde{A}(K')\tilde{A}(K'')\, e^{iX(K'+K'')}\, e^{-i\omega\tau(K'^2+K''^2)}(K'+K'')^2 \left[-\frac{\eta_1}{K'K''}\boldsymbol{e}_+ + \frac{\eta_2}{K'^2+K'K''+K''^2}\boldsymbol{e}_- \right] \right. \\
&\quad + 2\tilde{A}(K')\tilde{A}^*(K'')\, e^{iX(K'-K'')}\, e^{-i\omega\tau(K'^2-K''^2)}(K'-K'') \left[\frac{\eta_3}{K''}\boldsymbol{e}_+ - \frac{\eta_3^*}{K'}\boldsymbol{e}_- \right] \\
&\quad \left. + \tilde{A}^*(K')\tilde{A}^*(K'')\, e^{iX(-K'-K'')}\, e^{-i\omega\tau(-K'^2-K''^2)}(K'+K'')^2 \left[\frac{\eta_2^*}{K'^2+K'K''+K''^2}\boldsymbol{e}_+ + \frac{\eta_1^*}{K'K''}\boldsymbol{e}_- \right] \right\}.
\end{aligned}
\tag{B28}
$$

At $\mathcal{O}(\varepsilon^5)$, the relevant contributions arise from the combinations of the first term with A^* and from the second term with A. These read

$$
\begin{aligned}
2\begin{pmatrix} 3\bar{u}u_1u_2 \\ 3\bar{v}v_1v_2 \end{pmatrix} &= \frac{1}{2i\omega} \sum_{KK'K''} \tilde{A}^*(K)\tilde{A}(K')\tilde{A}(K'')\, e^{iX(-K+K'+K'')}\, e^{-i\omega\tau(-K^2+K'^2+K''^2)}(K'+K'')^2 \left[\frac{\eta_1}{K'K''}\boldsymbol{y}_1 + \frac{\eta_2}{K'^2+K'K''+K''^2}\boldsymbol{y}_2 \right] \\
&\quad + \frac{1}{i\omega} \sum_{KK'K''} \tilde{A}(K)\tilde{A}(K')\tilde{A}^*(K'')\, e^{iX(K+K'-K'')}\, e^{-i\omega\tau(K^2+K'^2-K''^2)}(K'-K'') \left[\frac{\eta_3}{K''}\boldsymbol{y}_2 - \frac{\eta_3^*}{K'}\boldsymbol{y}_1 \right] + \dots \\
&= \frac{1}{2i\omega} \sum_{KK'K''} \tilde{A}^*(K)\tilde{A}(K')\tilde{A}(K'')\, e^{iX(-K+K'+K'')}\, e^{-i\omega\tau(-K^2+K'^2+K''^2)} \\
&\quad \times \left\{ \left[\eta_1\frac{(K'+K'')^2}{K'K''} + 2\eta_3^*\frac{K'-K}{K'} \right]\boldsymbol{y}_1 + \left[\eta_2\frac{(K'+K'')^2}{K'^2+K'K''+K''^2} + 2\eta_3\frac{K'-K}{K} \right]\boldsymbol{y}_2 \right\}.
\end{aligned}
\tag{B29}
$$

Finally, we apply the Fredholm alternative, where only the combinations with $Q = K'$ and $K = K''$ or $Q = K''$ and $K = K'$ survive, and we again have to account for the overcounted contribution. We, therefore, obtain the additional contribution N_{qn} from the quadratic nonlinearity

$$
\begin{aligned}
N_{qn} &= \frac{1}{i\omega} \sum_Q Q^2\, e^{iQ\hat{X}}\tilde{A}(Q) \sum_K \tilde{A}(K)\tilde{A}^*(K) \left\{ \langle \boldsymbol{e}_+^\dagger; \boldsymbol{y}_1 \rangle \left[\eta_1\frac{(Q+K)^2}{QK} + \eta_3^*\frac{Q-K}{Q} \right] + \langle \boldsymbol{e}_+^\dagger; \boldsymbol{y}_2 \rangle \left[\eta_2\frac{(Q+K)^2}{Q^2+QK+K^2} + \eta_3\frac{Q-K}{K} \right] \right\} \\
&\quad - \frac{1}{2i\omega}(4\langle \boldsymbol{e}_+^\dagger; \boldsymbol{y}_1 \rangle\eta_1 + \frac{4}{3}\langle \boldsymbol{e}_+^\dagger; \boldsymbol{y}_2 \rangle\eta_2) \sum_Q Q^2\, e^{iQ\hat{X}}\tilde{A}(Q)|\tilde{A}(Q)|^2
\end{aligned}
\tag{B30}
$$

in the amplitude equation. Conceptually, these terms represent the proper contribution from the quadratic nonlinearity at $\mathcal{O}(\varepsilon^5)$. However, this is of little practical use, since these terms are both hard to analyze and to compute, arguably even more than the original dynamics. Therefore, one might consider further approximations (with or without asymptotical rigor) to obtain a proper contribution from the quadratic nonlinearity.

REFERENCES

[1] J. D. Crawford, "Introduction to bifurcation theory," Rev. Mod. Phys. **63**, 991–1037 (1991).

[2] M. C. Cross and P. C. Hohenberg, "Pattern formation out of equilibrium," Rev. Mod. Phys. **65**, 851–1112 (1993).

[3] R. B. Hoyle, *Pattern Formation—An Introduction to Methods* (Cambridge University Press, Cambridge, 2006).

[4] L. M. Pismen, *Patterns and Interfaces in Dissipative Dynamics*, Springer Series in Synergetics (Springer-Verlag, Berlin, 2023).

[5] H. Haken, *Synergetics: An Introduction*, Springer Series in Synergetics (Springer, 2012).

[6] P. C. Matthews and S. M. Cox, "Pattern formation with a conservation law," Nonlinearity **13**, 1293–1320 (2000).

[7] D. M. Winterbottom, P. C. Matthews, and S. M. Cox, "Oscillatory pattern formation with a conserved quantity," Nonlinearity **18**, 1031–1056 (2005).

[8] S. Ishihara, M. Otsuji, and A. Mochizuki, "Transient and steady state of mass-conserved reaction-diffusion systems," Phys. Rev. E **75**, 015203 (2007).

[9] U. Thiele, A. J. Archer, M. J. Robbins, H. Gomez, and E. Knobloch, "Localized states in the conserved Swift-Hohenberg equation with cubic nonlinearity," Phys. Rev. E **87**, 042915 (2013).

[10] M. Radszuweit, S. Alonso, H. Engel, and M. Bär, "Intracellular mechanochemical waves in an active poroelastic model," Phys. Rev. Lett. **110**, 138102 (2013).

[11] E. Bernitt, H. G. Dobereiner, N. S. Gov, and A. Yochelis, "Fronts and waves of actin polymerization in a bistability-based mechanism of circular dorsal ruffles," Nat. Commun. **8**, 15863 (2017).

[12] J. Halatek and E. Frey, "Rethinking pattern formation in reaction-diffusion systems," Nat. Phys. **14**, 507–514 (2018).

[13] J. Halatek, F. Brauns, and E. Frey, "Self-organization principles of intracellular pattern formation," Philos. Trans. R. Soc. London, Ser. B **373**, 20170107 (2018).

[14] C. Beta, N. S. Gov, and A. Yochelis, "Why a large-scale mode can be essential for understanding intracellular actin waves," Cells **9**, 1533 (2020).

[15] A. Yochelis, S. Flemming, and C. Beta, "Versatile patterns in the actin cortex of motile cells: Self-organized pulses can coexist with macropinocytic ring-shaped waves," Phys. Rev. Lett. **129**, 088101 (2022).

[16] T. Frohoff-Hülsmann and U. Thiele, "Nonreciprocal Cahn-Hilliard model emerges as a universal amplitude equation," Phys. Rev. Lett. **131**, 107201 (2023).

[17] I. S. Aranson and L. Kramer, "The world of the complex Ginzburg-Landau equation," Rev. Mod. Phys. **74**, 99–143 (2002).

[18] E. Knobloch, "Nonlocal amplitude equations," in *Pattern Formation in Complex Dissipative Systems*, edited by S. Kai (World Scientific, 1992), pp. 263–274.

[19] G. Schneider, "Justification of mean-field coupled modulation equations," Proc. R. Soc. Edinb. A: Math. **127**, 639–650 (1997).

[20] F. Bergmann, L. Rapp, and W. Zimmermann, "Active phase separation: A universal approach," Phys. Rev. E **98**, 020603 (2018).

[21] F. Bergmann and W. Zimmermann, "On system-spanning demixing properties of cell polarization," PLoS One **14**, e0218328 (2019).

[22] F. Brauns, J. Halatek, and E. Frey, "Phase-space geometry of mass-conserving reaction-diffusion dynamics," Phys. Rev. X **10**, 041036 (2020).

[23] F. Brauns, H. Weyer, J. Halatek, J. Yoon, and E. Frey, "Wavelength selection by interrupted coarsening in reaction-diffusion systems," Phys. Rev. Lett. **126**, 104101 (2021).

[24] G. Wolansky, "Multi-components chemotactic system in the absence of conflicts," Eur. J. Appl. Math. **13**, 641–661 (2002).

[25] K. John and M. Bär, "Travelling lipid domains in a dynamic model for protein-induced pattern formation in biomembranes," Phys. Biol. **2**, 123–132 (2005).

[26] A. Pototsky, U. Thiele, and H. Stark, "Mode instabilities and dynamic patterns in a colony of self-propelled surfactant particles covering a thin liquid layer," Eur. Phys. J. E **39**, 1–19 (2016).

[27] A. A. Nepomnyashchy and S. Shklyaev, "Longwave oscillatory patterns in liquids: Outside the world of the complex Ginzburg-Landau equation," J. Phys. A: Math. Theor. **49**, 053001 (2016).

[28] A. A. Nepomnyashchy and I. B. Simanovskii, "Novel criteria for the development of monotonic and oscillatory instabilities in a two-layer film," Phys. Fluids **29**, 092104 (2017).

[29] S. Takada, N. Yoshinaga, N. Doi, and K. Fujiwara, "Mode selection mechanism in traveling and standing waves revealed by min wave reconstituted in artificial cells," Sci. Adv. **8**, eabm8460 (2022).

[30] Z. H. You, A. Baskaran, and M. C. Marchetti, "Nonreciprocity as a generic route to traveling states," Proc. Natl. Acad. Sci. U.S.A. **117**, 19767–19772 (2020).

[31] S. Saha, J. Agudo-Canalejo, and R. Golestanian, "Scalar active mixtures: The non-reciprocal Cahn-Hilliard model," Phys. Rev. X **10**, 041009 (2020).

[32] T. Frohoff-Hülsmann, J. Wrembel, and U. Thiele, "Suppression of coarsening and emergence of oscillatory behavior in a Cahn-Hilliard model with nonvariational coupling," Phys. Rev. E **103**, 042602 (2021).

[33] T. Frohoff-Hülsmann and U. Thiele, "Localised states in coupled Cahn-Hilliard equations," IMA J. Appl. Math. **86**, 924–943 (2021).

[34] T. Frohoff-Hülsmann, U. Thiele, and L. M. Pismen, "Non-reciprocity induces resonances in a two-field Cahn-Hilliard model," Philos. Trans. R. Soc. A: Math. Phys. Eng. Sci. **381**, 20220087 (2023).

[35] T. Frohoff-Hülsmann, M. P. Holl, E. Knobloch, S. V. Gurevich, and U. Thiele, "Stationary broken parity states in active matter models," Phys. Rev. E **107**, 064210 (2023).

[36] D. Greve, G. Lovato, T. Frohoff-Hülsmann, and U. Thiele, "Coexistence of uniform and oscillatory states resulting from nonreciprocity and conservation laws," Phys. Rev. Lett. (in press); arXiv:2402.08634 (2024).

[37] T. Suchanek, K. Kroy, and S. A. M. Loos, "Irreversible mesoscale fluctuations herald the emergence of dynamical phases," Phys. Rev. Lett. **131**, 258302 (2023).

[38] T. Suchanek, K. Kroy, and S. A. M. Loos, "Time-reversal and parity-time symmetry breaking in non-hermitian field theories," Phys. Rev. E **108**, 064123 (2023).

[39] T. Suchanek, K. Kroy, and S. A. M. Loos, "Entropy production in the nonreciprocal Cahn-Hilliard model," Phys. Rev. E **108**, 064610 (2023).

[40] H. Alston, L. Cocconi, and T. Bertrand, "Irreversibility across a nonreciprocal PT-symmetry-breaking phase transition," Phys. Rev. Lett. **131**, 258301 (2023).

[41] F. Brauns and M. C. Marchetti, "Nonreciprocal pattern formation of conserved fields," Phys. Rev. X **14**, 021014 (2024).

[42] A. Förtsch, "Modellierung der Dynamik aktiver Teilchenmodelle in komplexer Umgebung und der universellen, kollektiven Dynamik gekoppelter, aktiver Spezies," Ph.D. thesis (Bayreuth, 2023).

[43] The fields u correspond to the real and imaginary part of a wave function ψ, i.e., the free-particle Schrödinger equation in its common form can be brought into this form via adding and subtracting its complex conjugate, $i\partial_t \psi = -\partial_{xx}\psi \quad \Leftrightarrow$
$$\partial_t \begin{pmatrix} \text{Im } \psi \\ \text{Re } \psi \end{pmatrix} = \begin{pmatrix} 0 & 1 \\ -1 & 0 \end{pmatrix} \partial_{xx} \begin{pmatrix} \text{Im } \psi \\ \text{Re } \psi \end{pmatrix}.$$

[44] In principle, other choices are possible. While exchanging the roles of $B(X)$ and $C(X)$ results in the equation for $A^*(X)$, keeping $B(X)$ arbitrary and $C(X) = 0$ will result in an evolution equation of type $\partial_T\langle B(X), A(X, T)\rangle = \ldots$. One could instead choose harmonics, i.e., $B(X) \sim e^{iQX}$ to first calculate projections of the amplitude onto single Fourier modes, and then construct the amplitude as their superposition. However, our choice already makes use of the complete null space, since the set of functions used for $B(X)$, i.e., $\{\delta(X - \hat{X}); \hat{X} \in [0, L]\}$ represents already a complete basis of the function space of periodic functions in $[0, L]$ and we, hence, already made use of the orthogonality to every element in the (infinite dimensional) null space of $\underline{L}^\dagger$.

[45] Note that exponentiating iH always results in the unitarity of e^{iH} for a Hermitian operator H. Further, here we can easily proof unitarity using Parseval's theorem, i.e., $\langle e^{i\omega\tau\partial_{XX}}A(X), e^{i\omega\tau\partial_{XX}}B(X)\rangle = \frac{1}{L}\int_0^L dX\left[e^{-i\omega\tau\partial_{XX}}A^\dagger(X)\right]\left[e^{i\omega\tau\partial_{XX}}B(X)\right]$
$= \sum_K \left[e^{i\omega\tau K^2}\tilde{A}^\dagger(K)\right]\left[e^{-i\omega\tau K^2}\tilde{B}(K)\right] = \sum_K \tilde{A}^\dagger(K)\tilde{B}(K) = \frac{1}{L}\int_0^L dX A^\dagger(X)B(X)$
$= \langle A(X), B(X)\rangle$.

[46] H. A. Dijkstra, F. W. Wubs, A. K. Cliffe, E. Doedel, I. F. Dragomirescu, B. Eckhardt, A. Y. Gelfgat, A. Hazel, V. Lucarini, A. G. Salinger, E. T. Phipps, J. Sanchez-Umbria, H. Schuttelaars, L. S. Tuckerman, and U. Thiele, "Numerical bifurcation methods and their application to fluid dynamics: Analysis beyond simulation," Commun. Comput. Phys. **15**, 1–45 (2014).

[47] S. Engelnkemper, S. V. Gurevich, H. Uecker, D. Wetzel, and U. Thiele, "Continuation for thin film hydrodynamics and related scalar problems," in *Computational Modeling of Bifurcations and Instabilities in Fluid Mechanics*, Computational Methods in Applied Sciences Vol. 50, edited by A. Gelfgat (Springer, Cham, 2019), pp. 459–501.

[48] H. Uecker, D. Wetzel, and J. D. M. Rademacher, "pde2path—A Matlab package for continuation and bifurcation in 2D elliptic systems," Numer. Math. Theory Methods Appl. **7**, 58–106 (2014).

[49] J. D. Crawford and E. Knobloch, "Symmetry and symmetry-breaking bifurcations in fluid dynamics," Ann. Rev. Fluid Mech. **23**, 341–387 (1991).

[50] M. Golubitsky and I. Stewart, "Hopf-bifurcation in the presence of symmetry," Arch. Ration. Mech. Anal. **87**, 107–165 (1985).

[51] A. Pototsky, M. Bestehorn, D. Merkt, and U. Thiele, "Morphology changes in the evolution of liquid two-layer films," J. Chem. Phys. **122**, 224711 (2005).

[52] M. Otsuji, S. Ishihara, C. Co, K. Kaibuchi, A. Mochizuki, and S. Kuroda, "A mass conserved reaction-diffusion system captures properties of cell polarity," PLoS Comput. Biol. **3**, e108 (2007).

05 December 2024 16:45:27

[53]J. Denk, S. Kretschmer, J. Halatek, C. Hartl, P. Schwille, and E. Frey, "MinE conformational switching confers robustness on self-organized Min protein patterns," Proc. Natl. Acad. Sci. U.S.A. **115**, 4553–4558 (2018).

[54]S. Kohyama, N. Yoshinaga, M. Yanagisawa, K. Fujiwara, and N. Doi, "Cell-sized confinement controls generation and stability of a protein wave for spatiotemporal regulation in cells," eLife **8**, e44591 (2019).

[55]M. Bonny, E. Fischer-Friedrich, M. Loose, P. Schwille, and K. Kruse, "Membrane binding of MinE allows for a comprehensive description of Min-protein pattern formation," PLoS Comput. Biol. **9**, e1003347 (2013).

[56]E. Knobloch, "Localized structures and front propagation in systems with a conservation law," IMA J. Appl. Math. **81**, 457–487 (2016).

[57]A. Förtsch and W. Zimmermann, "The universal CHEOPS, the path to it, and applications," in *Talk, DPG Spring Meeting, Dresden* (2023).

[58]E. Knobloch and J. De Luca, "Amplitude equations for traveling-wave convection," Nonlinearity **3**, 975–980 (1990).

[59]B. J. Matkowsky and V. Volpert, "Coupled nonlocal complex Ginzburg-Landau equations in gasless combustion," Physica D **54**, 203–219 (1992).

[60]W. Zimmermann, "Stability of traveling waves for a conserved field," Physica A **237**, 405–412 (1997).

[61]S. Saha and R. Golestanian, "Effervescent waves in a binary mixture with non-reciprocal couplings," arXiv:2208.14985 (2022).

[62]L. M. Pismen, "Selection of long-scale oscillatory convective patterns," Phys. Rev. A **38**, 2564–2572 (1988).

[63]D. Greve and U. Thiele (2024). "Data supplement for 'An amplitude equation for the conserved-Hopf bifurcation-Derivation, analysis, and assessment'," Zenodo. https://doi.org/10.5281/zenodo.14218246

05 December 2024 16:45:27